JOURNAL OF AGRICULTURAL AND FOOD CHEMISTRY



Functional Structure/Activity Relationships

# Identi#cation of Racemic and Chiral Carbazole Derivatives Containing an Isopropanolamine Linker as Prospective Surrogates Against Plant Pathogenic Bacteria: In Vitro and In Vivo Assays, and Quantitative Proteomics

Yong-Liang Zhao, Xing Huang, Li-Wei Liu, Peiyi Wang,
Qing-Su Long, Qing-Qing Tao, Zhong Li, and Song Yang

*J. Agric. Food Chem.*, **Just Accepted Manuscript** • DOI: 10.1021/acs.jafc.9b02036 • Publication Date (Web): 10 Jun 2019



## Just Accepted



is published by the American Chemical Society. 1155 Sixteenth Street N.W., Washington, DC 20036

# Identification of Racemic and Chiral Carbazole Derivatives Containing an Isopropanolamine Linker as Prospective Surrogates Against Plant Pathogenic Bacteria: *In Vitro* and *In Vivo* Assays, and Quantitative Proteomics

Yong-Liang Zhao [a], Xing Huang [a], Li-Wei Liu [a], Pei-Yi Wang* [a], Qing-Su Long [a], Qing-Qing Tao [a], Zhong Li [b], Song Yang* [a,b]

[a] State Key Laboratory Breeding Base of Green Pesticide and Agricultural Bioengineering, Key Laboratory of Green Pesticide and Agricultural Bioengineering, Ministry of Education, Center for R&D of Fine Chemicals of Guizhou University, Guiyang, 550025, China.

[b] College of Pharmacy, East China University of Science & Technology, Shanghai, China 200237.

* Corresponding authors.

E-mail: jhzx.msm@gmail.com (S. Yang), pywang888@126.com (P.-Y. Wang)

## Abstract

Recent observations on the emergence of drug-resistant plant pathogenic bacteria have highlighted and elicited an acute campaign to develop novel, highly efficient antibiotic surrogates for managing bacterial diseases in agriculture. Thus, a type of racemic and chiral carbazole derivative containing an isopropanolamine pattern was systematically synthesized to discover low-cost and efficient antibacterial candidates. Screening results showed that compounds **2f**, **6c**, and **2j** could significantly suppress the growth of tested plant pathogens, namely *Xanthomonas oryzae* pv. *oryzae*, *X. axonopodis* pv. *citri*, and *Pseudomonas syringae* pv. *actinidiae*, and provided the corresponding $EC_{50}$ values of 1.27, 0.993, and 0.603 μg/mL, which were extremely better than those of existing commercial drugs. *In vivo* study confirmed their prospective applications for controlling plant bacterial diseases. Label-free quantitative proteomics analysis indicated that compound **2f** could dramatically induce the up- and down-regulation of a total of 247 differentially expressed proteins, which was further validated by the parallel reaction monitoring technique. Moreover, fluorescence spectra and SEM images were performed to further explore the antibacterial mechanism.



## Keywords

carbazole, isopropanolamine, antibacterial, proteomics, action mechanism

45 **1. Introduction**

46 Despite the persistent threat posed by plant bacterial diseases and the identification of
47 a variety of widespread, highly phytopathogenic bacteria, the shortage of effective
48 antibacterial agents in agriculture causes considerable concern.[1-3] Currently, a limited
49 number of marketed bactericides, such as bismerthiazol (**BT**), thiodiazole copper
50 (**TC**), streptomycin (has been disabled for the risk potentials), triazoles, kocide, and
51 amobam, were exploited to manage these destructive bacterial diseases.[4,5] However,
52 these agents have performed reduced field control efficiency, not only due to their
53 long-term usage and abuse, but also ascribing to the single mode of action
54 performed.[6,7] Particularly, some of these pathogenic bacterial strains have
55 progressively experienced an elusive and prompt variation to acquire the flexible
56 defense mechanisms. Such complicated resistant pathogens can provide a quick and
57 adequate response against various existing external stimuli, putting agriculture in
58 considerable difficulty. For example, the application of marketed bactericide **BT** has
59 already resulted in the emergence of **BT**-resistant strains of *Xanthomonas oryzae* pv.
60 *oryzae* (*Xoo*) in Anhui Province, China.[2,4] Therefore, exploring and developing new
61 chemotherapeutic agents normally bearing different modes of action to combat
62 wild-type and drug-resistant pathogens is urgently required.

63 Elaborate observation found that agrochemicals, which can be commercialized
64 preferentially, possess the following features: simple structural architecture, short
65 synthetic procedures, facile operations for drug production, low manufacturing cost,
66 and superior biological activity. Concurrently, modern agricultural science has

proposed strict or even higher requirements, such as good biocompatibility and degradability, low residues, negligible phytotoxicity, permissible environmental friendliness, high selectivity for the target species, and low cytotoxicity toward non-target organisms, for the development of pesticide products. Therefore, the reasonable capture of a building block as the original template for exploring highly active antibacterial leads has elicited considerable concern. One of the effective sources for the selection is from the natural products in which the biological effects of various key skeletons have been carefully explored and highlighted. Carbazole skeleton with outstanding electronic and charge-transport properties has been frequently discovered and reported from many naturally occurring products.[8,9] Moreover, this privileged building block can be easily decorated with various functional groups, which endows carbazole-based derivatives and analogs with extensive and distinct biopharmaceutical activities, including antimicrobial,[10-14] anti-cancer,[15-17] insecticidal,[18,19] anti-viral,[20] anti-α-glucosidase,[21,22] anti-inflammatory,[23,24] anti-malarial,[25,26] anti-diabetic,[27,28] neuroprotective,[29,30] and anti-Alzheimer activities.[31-33] Given that the carbazole motif plays a crucial and versatile role in determining the final biological action of a target molecule, a large batch of natural and non-natural carbazole-tailored substrates acquiring prospective and practical applications in many fields, especially in the antimicrobial aspect, has also been presented.[8,34] As shown in Figure 1a, these kinds of typical natural carbazole derivatives were discovered to possess good antimicrobial effects against a wide range of medicinal bacteria and fungi including *Escherichia coli*, *Salmonella*

89 *typhi*, *Pseudomonas aeruginosa*, *Bacillus subtilis*, *Staphylococcus aureus*,
90 *Micrococcus luteus*, *Proteus vulgaris*, *Candida albicans*, and *Trichophyton*
91 *rubrum*.[35,36]

92 Considering the powerfully broad-spectrum bioactivity of carbazole-based
93 compounds, the relevant action mechanisms for their pharmaceutical effects have also
94 been extensively studied. Consequently, a variety of target species, such as diverse
95 enzymes or kinases (Pim-1 kinase, anaplastic lymphoma kinase, topoisomerase I, and
96 topoisomerase II), DNA, and G-quadruplexes (G-tetrads or G4-DNA), were
97 reported.[37-39] Inspired by the aforementioned studies, the rational design of title
98 compounds based on natural carbazole skeleton may probably lead to the discovery of
99 highly active antibacterial surrogates intended for the future battle against plant
100 bacterial diseases. Moreover, this kind of carbazole-tailored molecules may be
101 endowed with flexibly privileged functions for interacting with multiple targets of
102 pathogenic microorganisms, which probably reduces the risk of developing
103 bacteria-resistance. Few studies were performed to describe the general antibacterial
104 effects of carbazole-tailored compounds toward plant pathogens. Herein, a type of
105 simple racemic and chiral *N*-substituted carbazole derivative bridging by
106 isopropanolamine patterns (Figure 1b) was systematically synthesized and their
107 antibacterial effects were screened. In this study, three seriously invasive
108 phytopathogenic bacterial strains, including *Xoo*, *Xanthomonas axonopodis* pv. *citri*
109 (*Xac*), and *Pseudomonas syringae* pv. *actinidiae* (*Psa*), will be evaluated *in vitro*.
110 These pathogenic strains are known to cause destructive and widespread bacterial leaf

111 blight, citrus bacterial canker, and kiwifruit bacterial canker in agriculture, which
112 makes a mass of economic losses every year.[3,40,41] Subsequently, *in vivo* study will be
113 performed to verify the practical application for controlling bacterial diseases. In
114 addition, label-free quantitative proteomics and parallel reaction monitoring (PRM)
115 techniques, fluorescence spectra, and scanning electron microscopy (SEM) will be
116 utilized to study the possible antibacterial mechanism.

117 **2. Materials and methods**

118 **2.1 Instruments and Chemicals**

119 NMR spectra were obtained by using a Bruker Biospin AG-400 apparatus. Chemical
120 shifts were reported in parts per million (ppm) down field from TMS with the solvent
121 resonance as the internal standard. Coupling constants (*J*) were reported in Hz and
122 referred to apparent peak multiplications. SEM images were visualized and obtained
123 using Nova Nano SEM 450. Fluorescence spectra measurements were performed on a
124 Fluoromax-4 spectrofluorimeter (Horiba Trading CO., LTD).

125 **2.2 *In vitro* antibacterial bioassay (turbidimeter test)**

126 In our study, all the synthesized target compounds were evaluated for their
127 antibacterial activities against *Xoo*, *Xac*, and *Psa* by the turbidimeter test *in vitro*.[6]
128 Dimethylsulfoxide in sterile distilled water served as a blank control, Bismerthiazol
129 and Thiodiazole Copper served as positive controls. Approximately 40 μL of solvent
130 NB (1.5 g beef extract, 2.5 g peptone, 0.5 g yeast powder, 5.0 g glucose, and 500 mL
131 distilled water; pH = 7.0-7.2) containing *Xoo* (or *Xac*, or *Psa*), incubated on the phase
132 of logarithmic growth, was added to 5 mL of solvent NB containing different

133 concentrations of the test compounds and positive control, such as 20, 10, 5, 2.5, 1.25
134 μg/mL or 10, 5, 2.5, 1.25, 0.625 μg/mL (depending on the bioactivity of different
135 compounds, the concentrations were chosen in two times decline trend to make sure
136 the $EC_{50}$ values are inside the concentration ranges tested). The inoculated test tubes
137 were incubated at 28 ± 1 °C and continuously shaken at 180 rpm for 24-48 h until the
138 bacteria were incubated on the logarithmic growth phase. The growth of the cultures
139 was monitored on a microplate reader by measuring the optical density at 595 nm
140 ($OD_{595}$) given by turbidity corrected values = $OD_{\text{bacterial wilt}} - OD_{\text{no bacterial wilt}}$, and the
141 inhibition rate $I$ was calculated by $I = (C - T)/C \times 100\%$. C is the corrected turbidity
142 values of bacterial growth on untreated NB (blank control), and T is the corrected
143 turbidity values of bacterial growth on treated NB. By using the SPSS 17.0 software
144 and the obtained inhibition rates at different concentrations, a regression equation was
145 provided. The results of antibacterial activities (expressed by $EC_{50}$) against *Xoo*, *Xac*,
146 and *Psa* were calculated from the equation and the value was within the concentration
147 ranges. The experiment was repeated three times.

148 **2.3 *In vivo* bioassay against rice bacterial leaf blight**

149 The curative and protection activities of compound **2f** against rice bacterial leaf blight
150 were determined by Schaad's method with some slight modifications.[42] Bismerthiazol
151 (20% wettable powder) and thiodiazole copper (20% suspending agent), the
152 bactericides registered for rice bacterial leaf blight and purchased from the market,
153 served as the positive controls. The curative activity in potted plants for reducing rice
154 bacterial leaf blight of compound **2f** was determined under controlled conditions in a

155 growth chamber. After sowing the rice seeds of variety "Fengyouxiangzhan"
156 approximately 8 weeks, rice leaves were inoculated with *Xoo*, which was incubated at
157 logarithmic growth using sterilized scissors. One day after inoculation, **2f** solution at
158 200 μg/mL was uniformally sprayed onto the rice leaves until dripping down, whereas
159 distilled water was uniformally sprayed onto the negative control plants. Then, all
160 inoculated rice plants were placed in a plant growth chamber (28 °C and 90% RH). At
161 14 days after spraying, the disease index of the inoculated rice leaves was measured.
162 Similarly, the protection activity for reducing rice bacterial leaf blight of compound **2f**
163 was also conducted under controlled conditions. After sowing the rice seeds of variety
164 "Fengyouxiangzhan" approximately 8 weeks, compound **2f** solution at 200 μg/mL
165 was uniformally sprayed onto the rice leaves until dripping down, whereas distilled
166 water was uniformally sprayed onto the negative control plants. One day after
167 spraying, *Xoo*, which was incubated at logarithmic growth, was inoculated on the rice
168 leaves using sterilized scissors. All inoculated rice plants were placed in a growth
169 chamber (28 °C and 90% RH). At 14 days after inoculation, the disease index (C or T)
170 of the inoculated rice leaves was measured.[6] Firstly, the spot area of each leaf and the
171 whole leaf area were measured, and then the percentage of the spot area in the whole
172 leaf area was calculated. Secondly, these leaves were classed according to the
173 following grading standards. Grade 1: the area of disease spot accounts for less than
174 5% of the whole leaf area; Grade 3: the area of disease spot accounts for 6-10% of the
175 whole leaf area; Grade 5: the area of disease spot accounts for 11-20% of the whole
176 leaf area; Grade 7: the area of disease spot accounts for 21-50% of the whole leaf

177 area; Grade 9: the area of disease spot accounts for more than 50% of the whole leaf
178 area. Finally, the disease index (C or T) was calculated using the following formula:
179 Disease index (C or T) = $\sum$(the number of leaves at each Grade × the corresponding
180 Grade) / (the total number of leaves × the superlative Grade).

181 The control efficiencies *I* for the curative and protection activities are calculated
182 by the following equation: Control efficiency *I* (%) = (C - T) / C ×100. In the
183 equation, C is the disease index of the negative control and T is the disease index of
184 the treatment group.

185 **2.4 Label-free quantitative proteomics analysis**

186 **2.4.1 Bacterial strains and growth conditions**

187 The bacterial strain used in this study was *Xoo*, which is the causative pathogen of
188 rice bacterial leaf blight. The *Xoo* was cultivated in liquid nutrient broth medium (1.5
189 g beef extract, 2.5 g peptone, 0.5 g yeast powder, 7.5 g sucrose, added into 500 mL
190 distilled water, pH 7.0–7.2) at 28–30°C for 12 h. Cells were harvested when $OD_{600}$
191 (optical density at 600 nm) reached approximately 0.1. Then compound **2f** with the
192 concentration of 6.35 μg/mL (5×$EC_{50}$) was added into the mixture and cultured at
193 28-30 °C. When the $OD_{600}$ of the control group reached to 0.6-0.8, all the samples
194 were collected and centrifuged at 8000 rpm at 4 °C, respectively. Three biological
195 replicates were prepared for each condition.

196 **2.4.2 Protein extraction and trypsin digest**

197 The extraction of all *Xoo* proteins were performed based on the methods with a slight
198 modification.[43] Briefly, the sample was sonicated three times on ice using a high

199 intensity ultrasonic processor (Scientz) in lysis buffer (8 M urea, 1% Protease
200 Inhibitor Cocktail). The remaining debris was removed by centrifugation at 12,000 g
201 at 4 °C for 10 min. Finally, the supernatant was collected and the protein
202 concentration was determined with BCA kit according to the manufacturer's
203 instructions. For digestion, the protein solution was reduced with 5 mM dithiothreitol
204 for 30 min at 56 °C and alkylated with 11 mM iodoacetamide for 15 min at room
205 temperature in darkness. The protein sample was then diluted to a urea concentration
206 (less than 2 M). Finally, the trypsin was added into the protein sample by 1:50
207 trypsin-to-protein mass ratio for the first digestion overnight, and 1:100
208 trypsin-to-protein mass ratio for a second 4 h-digestion.

209 **2.4.3 LC-MS/MS analysis**

210 The tryptic peptides were dissolved in 0.1% formic acid, directly loaded onto a
211 home-made reversed-phase analytical column (15 cm length, 75 μm i.d.). The
212 gradient was comprised of an increase from 6% to 23% (0.1% formic acid in 98%
213 acetonitrile) over 26 min, 23% to 35% in 8 min and climbing to 80% in 3 min, then
214 holding at 80% for the last 3 min, all at a constant flow rate of 400 nL/min on an
215 EASY-nLC 1000 UPLC system.

216 The peptides were subjected to NSI source followed by tandem mass
217 spectrometry (MS/MS) in Q ExactiveTM Plus (Thermo) coupled online to the UPLC.
218 The electrospray voltage applied was 2.0 kV. The m/z scan range was 350 to 1800 for
219 full scan, and intact peptides were detected in the Orbitrap at a resolution of 70,000.
220 Peptides were then selected for MS/MS using NCE setting as 28 and the fragments

221 were detected in the Orbitrap at a resolution of 17,500. A data-dependent procedure
222 that alternated between one MS scan followed by 20 MS/MS scans with 15.0 s
223 dynamic exclusion. Automatic gain control (AGC) was set at 50000. Fixed first mass
224 was set as 100 m/z.

225 **2.4.4 Protein identification**

226 The resulting MS/MS data were processed using Maxquant search engine (v.1.5.2.8).
227 Tandem mass spectra were searched against *Xoo* database concatenated with reverse
228 decoy database. Trypsin/P was specified as cleavage enzyme allowing up to 2 missing
229 cleavages. The mass tolerance for precursor ions was set as 20 ppm in First search and
230 5 ppm in Main search, and the mass tolerance for fragment ions was set as 0.02 Da.
231 Carbamidomethyl on Cys was specified as fixed modification and oxidation on Met
232 was specified as variable modifications. The false discovery rate (FDR) for peptide
233 and protein identifications was set to 0.01 and minimum score for peptides was
234 set >40. It should be combined and reported as one protein group to identify peptides
235 which all appear between two proteins. We used label-free quantification with a
236 minimum of two ratio counts to determine the normalized protein intensity to
237 compare between samples. We used the iBAQ algorithm to rank the absolute
238 abundance of different proteins within a single sample. Protein tables were filtered to
239 eliminate the interference from common contaminants and reverse database. A
240 two-sample unpaired t-test was used to identify the differentially accumulated
241 proteins between control and treatment groups. The iBAQ data were used for the
242 t-test, and proteins with p value $\leqslant 0.05$ were considered differentially expressed.

243 **2.4.5 Bioinformatics analysis**

244 Gene Ontology (GO) annotation proteome was derived from the UniProt-GOA
245 database (www. http://www.ebi.ac.uk/GOA/). Firstly, Converting identified protein
246 ID to UniProt ID and then mapping to GO IDs by protein ID. If some identified
247 proteins were not annotated by UniProt-GOA database, the InterProScan soft would
248 be used to annotated protein's GO functional based on protein sequence alignment
249 method. GO items can be divided into three categories, namely, biological process
250 (BP), cellular components (CC), and molecular functions (MF). In this study, we
251 mapped the differentially displayed proteins (fold changes >1.5, P<0.05) into the GO
252 database (http://www.geneontology.org/). It was computable for the amount of
253 proteins at each GO term, and the target list used for result which came from
254 label-free. The list was constructed by downloading the data on the GO database.
255 Kyoto Encyclopedia of Genes and Genomes (KEGG) database was used to annotate
256 protein pathway. Firstly, using KEGG online service tools KAAS to annotated
257 protein's KEGG database description. Then mapping the annotation result on the
258 KEGG pathway database used KEGG online service tools KEGG mapper.

259 **2.5 Fluorescence analysis**

260 The total DNA was isolated from *Xoo* by TIANamp bacterial DNA kit. The
261 concentration of DNA was determined by UV absorption at 260 nm using a molar
262 absorption coefficient $\xi_{260}$ = 6600 L $mol^{-1}$ $cm^{-1}$ (expressed as molarity of phosphate
263 groups) by Bouguer-Lambert-Beer law. The purity of DNA was checked by
264 monitoring the ratio of the absorbance at 260 nm to that at 280 nm. The solution gave

265 a ratio of >1.8 for $A_{260}/A_{280}$, which indicated that DNA was sufficiently free from
266 protein. Then compound **2f** was added into a TRIS-HCl buffer solution (50 nM, pH =
267 7.4) containing different amounts of DNA. The final volume was fixed to 10 mL and
268 the final concentration of compound **2f** was $1\times10^{-8}$ mol $L^{-1}$. After incubating the
269 solution for 20 min at room temperature, fluorescence spectra were recorded on
270 F-7000 Spectrofluorimeter (Hitachi, Tokyo, Japan) equipped with 1.0 cm quartz cells,
271 the widths of both the excitation and emission slit were fixed as 5 nm, and the
272 excitation wavelength was 363 nm.

273 **2.6 Scanning electron microscopy (SEM)**

274 In this assay, 1.5 mL *Xoo* (or *Xac* or *Psa*) cells incubated at the logarithmic phase
275 were centrifuged and washed with PBS (pH = 7.2), and re-suspended in 1.5 mL of
276 PBS buffer (pH = 7.2). After that, bacteria *Xoo* (or *Xac* or *Psa*) were incubated with
277 compound **2f** at concentrations of 12.5 μg/mL, 25.0 μg/mL, and an equivalent volume
278 of DMSO (solvent control) for 6 h at room temperature. After incubation, these
279 samples were washed 3 times with PBS (pH = 7.2). Subsequently, the bacterial cells
280 were fixed for 8 h at 4 ℃ with 2.5% glutaraldehyde, and then dehydrated with graded
281 ethanol series and pure tert-butanol (2 times with 10 min/time). Following
282 dehydration, samples were freezing dried and coated with gold, and visualized using
283 Nova Nano SEM 450.

284 **3. Results and Discussion**

285 An isopropanolamine linker was elaborately investigated and will be integrated into
286 the title compounds to efficiently fabricate a type of simple carbazole derivative,

287 which probably possesses adequate competence to inhibit the growth of plant
288 pathogens; this linker has been extensively exploited as a versatile tool or bridge to
289 construct pharmacological substrates, which displayed impressive biological activities
290 in many fields.[14,34] Therefore, a series of carbazole compounds bridging by this
291 isopropanolamine linker was synthesized following Figure 2. Briefly, carbazole was
292 treated with racemic epichlorohydrin under strong alkali conditions of KOH to give
293 the key intermediate **1** bearing an epoxy tail, which was subsequently ring-opened by
294 various substituted benzylamines to afford title molecules **2a–2k**. All these racemic
295 molecular structures were confirmed by $^{1}$H NMR, $^{13}$C NMR, and HRMS. For their
296 antibacterial evaluation, the typical turbidimeter test was conducted, while the mainly
297 used agricultural agents **BT** and **TC** were co-assayed as reference drugs. As indicated
298 in Table 1, most of the designed compounds displayed significant antibacterial powers
299 against the tested three bacterial strains. For anti-*Xoo* and anti-*Xac* activity, numerous
300 compounds provided the corresponding $EC_{50}$ values ranging from 1.39 to 4.30 μg/mL
301 and 1.80 to 2.54 μg/mL except compounds **2d** and **2g**, which afforded relatively high
302 $EC_{50}$ values of 10.2, 35.4 μg/mL and 8.01, 30.5 μg/mL, respectively. For anti-*Psa*
303 assays, these compounds also showed outstanding performances in suppressing the
304 pathogen growth with $EC_{50}$ values within 0.603 and 29.7 μg/mL apart from
305 compounds **2d** and **2i**, which presented the negligible antibacterial ability with $EC_{50}$
306 values exceeding 100 μg/mL. The above findings indicated that the design of
307 carbazole-based compound bridging by the isopropanolamine linker could promote
308 the discovery of highly efficient molecules probably applied in agriculture. The

309 structure–activity relationship (SAR) was elucidated according to the obtained $EC_{50}$
310 values and the effect of different substituents on the benzene ring. The electronic
311 property, the type of halogens, the position, and steric hindrance of substituents
312 clearly have a significant influence toward the bioactivity. Compared with
313 unsubstituted compound **2c** ($EC_{50}$ values of 2.76, 2.46, 3.94 μg/mL against *Xoo*, *Xac*,
314 and *Psa*, respectively), introducing a weak electron-donating group 4–$CH_3$ (**2b**, 1.51,
315 1.80, and 3.73 μg/mL) or weak electron-withdrawing groups 4-Cl (**2f**, 1.27, 1.96, and
316 3.83 μg/mL) or 4-F (**2j**, 2.04, 2.42, and 0.603 μg/mL) would improve the bioactivity.
317 Notably, the antibacterial effects on *Psa* were increased by approximately two folds
318 after introducing a strong electron-donating group (4-$OCH_3$, **2a**, 1.79 μg/mL) and
319 were reduced by approximately two folds after placing a strong electron-withdrawing
320 group (4-$CF_3$, **2k**, 9.24 μg/mL) on the benzene ring. Appreciably, the position of the
321 substituents provided different tendencies toward the three strains. For anti-*Xoo*
322 activity, the order of activities followed para (R = 4-Cl or 4-F, **2f** and **2j**, 1.27 and
323 2.04 μg/mL) > ortho (R = 2-Cl or 2-F, **2d** and **2h**, 10.2 and 4.30 μg/mL). By contrast,
324 different patterns were observed for the anti-*Xac* activity, providing the results of para
325 (R = 4-Cl, **2f**, 1.96 μg/mL) > ortho (R = 2-Cl, **2d**, 8.01 μg/mL). Additionally, the
326 substituent located at the para-position afforded the most powerful potency against
327 *Psa* with the $EC_{50}$ value of 0.603 μg/mL (4-F, **2j**). In another aspect, a remarkable
328 observation indicated that the antibiotic action was dramatically decreased after
329 introducing an additional steric group on the benzene ring, which was illustrated by
330 comparing the bioactivity of compounds **2f** (4-Cl, 1.27, 1.96, 3.83 μg/mL) and **2g**

331 (2,4-diCl, 35.4, 30.5, 29.7 μg/mL). From the above results, admirable antibacterial
332 effects with the minimal $EC_{50}$ values of 1.27, 1.80, and 0.603 μg/mL against the
333 corresponding strains of *Xoo*, *Xac*, and *Psa* were achieved.

334 Further modification from various aspects was conducted based on the preceding
335 study to explore even superior bioactive molecules. First, influence of replacing the
336 benzene ring into the heterocyclic scaffolds on the antibacterial effect was examined,
337 and compounds **2l**, **2m**, and **2n** bearing furan, thiofuran, or pyridine moieties were
338 prepared. Although these compounds still performed strong inhibition powers against
339 the three pathogens with $EC_{50}$ values ranging from 2.06 to 7.23 μg/mL, except for
340 compound **2m** against *Psa* ($EC_{50}$ value > 100 μg/mL), they could not afford a better
341 antibacterial action. Second, substituted arylamines were employed to ring-open the
342 epoxy motif instead of substituted benzylamines and resulted in the fabrication of title
343 compounds **2o–2r**. Even though compounds **2p** and **2r** provided a tolerable inhibition
344 action toward *Psa* with the corresponding $EC_{50}$ values of 12.2 and 32.0 μg/mL, the
345 antibacterial effects of these compounds were significantly blocked after removing the
346 methylene group. This finding suggested that ring-opening the epoxy motif with a
347 relatively flexible and relaxed amine would be beneficial to the bioactivity. A series
348 of title compounds (**2s–2x**) bearing the saturated alkyl amine motifs were synthesized
349 to verify this hypothesis and their bioactivities were tested. Notably, the $EC_{50}$ values
350 of these compounds experienced three steps of variation tendencies: first, increasing
351 to extend the alkyl chain length, suggesting that slightly raising the hydrophobicity of
352 title compounds was disadvantageous to the activity; then being decreased after

353 introducing a long alkyl chain (for example, n-butyl, **2w**, providing the minimal $EC_{50}$
354 values of 2.09, 1.90, and 4.84 μg/mL against *Xoo*, *Xac*, and *Psa*, respectively),
355 indicating that the title molecule bearing a providential and adjustable lipophilic tail
356 would elevate the antibacterial potency; finally, elevation along with the introduction
357 of a sterically hindered group (tert-butyl, **2x,** providing $EC_{50}$ values of 7.34, 12.5, and
358 5.55 μg/mL against *Xoo*, *Xac*, and *Psa*, respectively), indicating that a bulk group
359 located at the molecular tail would block the additional interactions with target
360 species. Based on the preceding modification and obtained bioassay results, even
361 slight changes in the molecular patterns would significantly affect the final
362 bioactivity. Therefore, molecular framework maps must be carefully and
363 systematically optimized.

364 Given that compounds **2f**, **2b**, and **2j** bearing the corresponding 4-chlorobenzyl,
365 4-methylbenzyl, and 4-fluorobenzyl groups exerted the best antibacterial potency
366 against *Xoo* ($EC_{50}$ = 1.27 μg/mL), *Xac* ($EC_{50}$ = 1.80 μg/mL), and *Psa* ($EC_{50}$ = 0.603
367 μg/mL), respectively, the substituents on the carbazole ring toward bioactivity were
368 investigated. Therefore, compounds **4a–4h** bearing 3,6-diBr, 3,6-ditert-butyl, or
369 3,6-diacetyl motifs were prepared (Figure 3) and biologically evaluated. As shown in
370 Table 2, the anti-*Psa* activity was significantly decreased after introducing the
371 substituents on the carbazole ring and resulted in the $EC_{50}$ values exceeding 100
372 μg/mL, suggesting that the additional substituted groups could seriously block the
373 interactions with *Psa* target species. For anti-*Xoo* and anti-*Xac* activity, an increased
374 pharmacological effect was observed via the introduction of the 3,6-diBr moiety (**4c**)

375 and provided the corresponding $EC_{50}$ values of 1.10 and 1.62 μg/mL. By contrast, an
376 opposite pattern was observed from $EC_{50}$ values of compounds **4a** (17.9 and >100
377 μg/mL) and **4b** (17.2 and >100 μg/mL), indicating that an electron-donating group
378 (-$CH_3$, **4c**) on the benzene ring was beneficial to bioactivity in comparison to those
379 weak electron withdrawing groups (4-Cl, **4a**; 4-F, **4b**). Notably, introducing a
380 hydrophobic and bulk group (3,6-ditert-butyl, **4d-4f**) led to a comparative activity
381 toward *Xoo* and slightly improved efficiency toward *Xac*, respectively. By contrast,
382 the introduction of 3,6-diacetyl motif (**4g** and **4h**) significantly reduced the
383 antibacterial potency, demonstrating that an electron-withdrawing group was
384 unfavorable to the bioactivity. Given the preceding results, the antibacterial
385 competence could be affected by various substituents on the carbazole ring, which
386 provides a new template and guidance for the careful optimization of the molecular
387 framework.

388 After evaluating the antibacterial effect of substituents on the carbazole ring, the
389 absolutely chiral carbazole derivatives toward activity must be clarified. Therefore, **6a**
390 (*R*), **6b** (*S*), **6c** (*R*), and **6d** (*S*) were synthesized by replacing the racemic
391 epichlorohydrin into the corresponding chiral material (Figure 4). Bioassay results
392 indicated that the fixed configuration had certain effects toward the antibacterial
393 efficiency (Table 3). For the anti-*Xoo* activity, their $EC_{50}$ values presented the
394 following order, *R*-forms (1.38 μg/mL, **6a**; 0.902 μg/mL, **6c**) < *R/S*-forms (1.47
395 μg/mL, **4d**; 1.32 μg/mL, **4f**) < *S*-forms (1.51 μg/mL, **6b**; 1.43 μg/mL, **6d**), suggesting
396 that the *R*-forms of target compounds were beneficial to bioactivity. For anti-*Xac*

397 bioassay, a distinct pattern was provided as $R_1$ = 4-chlorobenzyl, and their $EC_{50}$
398 values followed the order of *R/S*-form (2.42 μg/mL, **4d**) < *S*-form (3.11 μg/mL, **6b**) <
399 *R*-form (5.49 μg/mL, **6a**). This finding indicates that the combination of *S*- and
400 *R*-form can improve the antibacterial power. Based on the preceding investigation, the
401 final bioactivity could be affected by the absolute configuration of the chiral center in
402 the designed molecular structure.

403 *In vivo* studies were conducted to fight against rice bacterial leaf blight and
404 estimate the prospective applications of this kind of compounds against plant bacterial
405 diseases. In this study, compound **2f** was selected due to its superior anti-*Xoo* activity
406 (1.27 μg/mL) and accessibility for synthesis. As shown in Table 4 and Figure 5,
407 compound **2f** exhibited good *in vivo* curative and protection activities toward bacterial
408 leaf blight diseases with the corresponding control efficiency of 50.77% and 48.71%
409 at 200 μg/mL, respectively, which were superior to those of **BT** (43.47% and 40.91%)
410 and **TC** (42.60% and 39.17%). This outcome suggests that this type of molecular
411 structure can be considered as a template for the future exploration and development
412 of highly efficient alternatives.

413 A label-free quantitative proteomic analysis was conducted in response to the
414 compound **2f** stimulation to examine the underlying antibacterial mechanism of this
415 type of designed compound toward *Xoo*. In this study, three biological replicates were
416 conducted for each group (**2f** and **CK**) to ensure the reliability of the results (detected
417 by relative standard deviation (RSD) analysis, Figure 6a) and the total proteins of
418 samples were identified through label-free LC-MS/MS. The result showed that a total

419 of 2337 proteins were preliminary monitored for **CK** and **2f** samples, among which
420 2095 proteins with quantitative information were identified (Table S1). Comparing
421 the treatment (**2f**) and control (**CK**) groups, 1848 proteins (88.2%) presented common
422 expression levels, while 247 proteins (100 up-regulated, 147 down-regulated; fold
423 changes > 1.5, $p < 0.05$) were confirmed differentially expressed (Table S2, Figure
424 6b). A volcano plot map was also utilized to filter the significant differentially
425 expressed proteins (Figure 6c). This outcome indicates that compound **2f** could
426 significantly provoke the pathogen to provide a physiological response against the
427 external stimulus, and consequently produced a series of differentially expressed
428 proteins.

429 These differentially expressed proteins were analyzed for GO categories in
430 biological process (BP), molecular function (MF), and cellular component (CC) to
431 preliminarily clarify their biological functions.[43-45] According to their BP (Figure 7A),
432 a large proportion of these proteins were clearly involved in the metabolic process,
433 localization, cellular process, and single-organism process. Figure 7B showed that a
434 large quantity of these differentially expressed proteins was involved in catalytic
435 activity, binding transporter activity on the basis of their MF. Meanwhile, CC analysis
436 showed that most of these proteins were found in membrane and cell (Figure 7C).
437 Moreover, the subcellular localization chart revealed that most of these differentially
438 expressed proteins were mainly found in the cytoplasmic (Figure Sa). Clusters of
439 Orthologous Groups (COG) chart was exploited to further expound the functional
440 classification of these unique proteins.[46] As indicated in Figure Sb, 21 representative

441 functions, such as "Energy production and conversion," "Amino acid transport and
442 metabolism," "Carbohydrate transport and metabolism," "Lipid transport and
443 metabolism," "Cell wall/membrane/envelope biogenesis," and "General function
444 prediction only", were predicted. This observation suggests that a variety of
445 physiological processes could be dramatically influenced and triggered by the
446 stimulation from compound **2f**.

447 The KEGG pathway enrichment bubble plot chart (Figure Sc) was presented to
448 determine the receivable action pathways containing multiple differentially expressed
449 proteins induced by compound **2f**.[47] Two main metabolic pathways containing biotin
450 metabolism pathway and starch and sucrose metabolism pathway involving additional
451 differentially expressed proteins were locked. The two pathways are known to play
452 one of the key approaches in the biosynthesis of biotin and D-glucose, which are
453 normally participants in a variety of physiological processes including more than the
454 metabolisms of fat, protein, and energy. The disturbance or blockage of the access
455 will result in serious problems, such as delayed growth, energy deficiency, and
456 biochemical disorder.[48,49] In the biotin metabolism pathway (Figure 8), the
457 harmonious cooperation of these proteins is essential for the normal operation.
458 However, an array of down-regulated proteins was observed in this pathway. For
459 example, beta-ketoacyl-synthase I (Fab B) and 3-oxoacyl-(Acyl-carrier-protein)
460 reductase (Fab G) are the main enzymes performing significant roles in the
461 biosynthesis of fatty acid; by contrast, the expression quantity of biotin synthase
462 (2.8.1.6), ATP-dependent dethiobiotin synthetase BioD (6.3.3.3), and

463 8-amino-7-oxononanoate synthase (2.3.1.47) would further influence the synthesis of
464 biotin. Simultaneously, in the starch and sucrose metabolism pathway, the evidently
465 decreased expression of beta-glucosidase (3.2.1.21) might directly lead to the reduced
466 conversion of GDP-glucose into D-glucose, which would disrupt the normal energy
467 metabolism of bacteria and consequently resulted in the failure of normal life
468 activities of bacteria. By contrast, the up-regulated proteins, including endoglucanase
469 (3.2.1.4), trehalose-6-phosphate synthase (2.4.1.15), and trehalose 6-phosphate
470 phosphatase (3.1.3.12), would cause the imbalance of these key metabolic
471 intermediates, further breaking the normal pathway metabolism. This outcome
472 suggested that compound **2f** might have the privileged competence to induce the
473 expression of differential proteins affecting the crucial metabolic pathways, and
474 consequently resulted in the disorder of normal physiological processes and final
475 bacteria death.

476 Protein–protein interaction networks were presented using STRING database
477 version 10.5 to further study and assign the function and association of these
478 differentially expressed proteins. As indicated in Figure 9, 12 functions, including
479 "Fatty acid biosynthesis," "Translation ribosomal structure and biogenesis," "Lipid
480 transport and metabolism," "RNA processing and modification," "Ion transport and
481 metabolism," "Amino acid transport and metabolism," "Phosphotransferase system,"
482 "Nucleotide transport and metabolism," "Cytochrome oxidoreductase,"
483 "Oxidoreductase," "Biotin metabolism," and "Starch and sucrose metabolism" were
484 enriched. This finding further suggested that various physiological processes could be

485 significantly affected by compound **2f** stimulation and consequently led to the
486 disturbance and final bacteria death.

487 PRM technique was performed to further validate the label-free quantitative
488 proteomics result, because it is another widely used and efficient method which can
489 precisely quantify and verify an array of target proteins of interest.[50-52] In this study,
490 twenty significant differentially produced proteins involved in these GO terms and
491 pathways were selected for PRM analysis (Table S3). Moreover, two unique peptides
492 with anticipated chemical stability were chosen for each protein, and the relative
493 protein abundance was expressed as the average of the two normalized peptide peak
494 areas (Table S4). The PRM result was shown in Figure 10 and afforded the same
495 trends with the label-free quantitative proteomics data.

496 The natural carbazole scaffold is known to normally possess the privileged
497 ability to interact with DNA, which results in changes in fluorescence intensity.[13,34]
498 Fluorescence spectrometry was used to monitor the interactions between the total
499 DNA extracted from pathogen *Xoo* and compound **2f**. Primarily, time dependent
500 fluorescent intensity of compound **2f** in the TRIS-buffer revealed that the fluorescence
501 was constant after 20 min (Figure 11a). After the addition of an equivalent DNA, the
502 fluorescent intensity was first decreased, and then became constant for 20 min
503 incubation (Figure 11b). This outcome might be attributed to the encapsulation of the
504 carbazole moiety into the grooves of DNA helical structures, and consequently
505 reduced the total amount of carbazoles to produce fluorescence. A gradually
506 decreased fluorescent intensity for compound **2f** with different dosages of DNA

507 further confirmed that the designed compounds bearing carbazole patterns had strong
508 interactions with the DNA of pathogens (Figure 11c), which was in accordance with
509 the observation of differentially expressed proteins.

510 The SEM images of *Xoo*, *Xac*, and *Psa* were presented to study the morphology
511 changes after being subjected to different dosages of compound **2f**. As indicated in
512 Figure 12, the shapes of these pathogens were changed from well-proportioned
513 (Figures 12a, 12d, and 12g) to partially corrugated or broken (Figures 12b, 12e, and
514 12h) after treatment with compound **2f** at the dosage of 12.5 μg/mL. Furthermore,
515 nearly all these pathogens were destroyed when the drug concentration was elevated
516 to 25 μg/mL and consequently afforded the observation of various debris and large
517 leakage holes on the bacteria surfaces (Figures 12c, 12f, and 12i). This result further
518 confirmed that the designed compounds performed strong interactions with the target
519 species of bacteria, which subsequently led to a series of physiological process
520 changes and final bacteria death.

521 In summary, a type of simple racemic and chiral carbazole derivative possessing
522 an isopropanolamine pattern was systematically synthesized and evaluated their
523 antibacterial activities. Bioassay results showed that compounds **2f**, **6c**, and **2j** could
524 evidently inhibit the growth of plant pathogens *Xoo*, *Xac* and *Psa* with the
525 corresponding $EC_{50}$ values of 1.27, 0.993, and 0.603 μg/mL, which were extremely
526 superior to those of **BT** (92.6 μg/mL) and **TC** (121.8, 77.0, and 87.0 μg/mL).
527 Moreover, the SAR analysis indicated that the electronic property, the type of
528 halogens, the position, steric hindrance of substituents, and molecular absolute

529 configuration had a dramatic influence toward the bioactivity. *In vivo* study confirmed
530 the prospective application for developing these compounds as agricultural agents
531 against plant bacterial diseases. Quantitative proteomics analysis indicated that
532 compound **2f** could induce a total of 247 proteins (100 up-regulated, 147
533 down-regulated) differentially expressed comparing to the negative control, which
534 was further validated by the PRM result. This occurrence significantly affected
535 various physiological processes of pathogens and eventually resulted in their
536 morphological variations from SEM images. Moreover, fluorescence spectra
537 suggested that this kind of compounds had strong interactions with the DNA of
538 pathogens. Considering their privileged features and multi-interactions with the target
539 species of tested pathogens, these versatile carbazole derivatives could be considered
540 as a suitable template for exploring highly efficient antibacterial surrogates against
541 plant bacterial infections and disabling the bacterial resistance.

542 **Acknowledgment**

543 We acknowledge the financial support of National Natural Science Foundation of
544 China (21877021, 21662009, 21702037, 31860516), the Research Project of Ministry
545 of Education of China (20135201110005, 213033A), and Guizhou Provincial S&T
546 Program ([2012]6012, LH [2017]7259, [2017]5788).

547 **Supporting Information**

548 Supplementary data including experimental procedures for PRM, partial racemic or
549 chiral intermediates and target compounds were analyzed by HPLC (Figures S1-S10),
550 Figures Sa-Sc, Tables S1-S5, synthetic procedures for the intermediates and target

compounds and $^{1}H$ NMR, $^{13}C$ NMR, and HRMS spectra of target compounds associated with this article can be found, in the online version, at https://pubs.acs.org/journal/jafcau.

**Conflict of interest**

The authors declare no competing financial interest.

557 **Reference**

558 (1) Hou, Z.; Zhu, L. F.; Yu, X. C.; Sun, M. Q.; Miao, F.; Zhou, L. Design, Synthesis,
559 and Structure-Activity Relationship of New 2-Aryl-3, 4-dihydro-*β*-carbolin-2-ium
560 Salts as Antifungal Agents. *J. Agric. Food Chem*. **2016**, *64*, 2847-2854.
561 (2) Dang, Q. L.; Kim, W. K.; Nguyen, C. M.; Choi, Y. H.; Choi, G. J.; Jang, K. S.;
562 Park, M. S.; Lim, C. H.; Ngoc, H. L.; Kim, J. C. Nematicidal and Antifungal
563 Activities of Annonaceous Acetogenins from *Annona squamosa* against Various
564 Plant Pathogens. *J. Agric. Food Chem.* **2011**, *59*, 11160-11167.
565 (3) Jian, W. L.; He, D. H.; Xi, P. G.; Li, X. W. Synthesis and Biological Evaluation
566 of Novel Fluorine-Containing Stilbene Derivatives as Fungicidal Agents against
567 Phytopathogenic Fungi. *J. Agric. Food Chem.* **2015**, *63*, 9963-9969.
568 (4) Li, P.; Shi, L.; Gao, M. N.; Yang, X.; Xue, W.; Jin, L. H.; Hu, D. Y.; Song, B. A.
569 Antibacterial activities against rice bacterial leaf blight and tomato bacterial wilt
570 of 2-mercapto-5-substituted-1,3,4-oxadiazole/thiadiazole derivatives. *Bioorg.*
571 *Med. Chem. Lett.* **2015**, *25*, 481-484.
572 (5) Wang, P. Y.; Zhou, L.; Zhou, J.; Wu, Z. B.; Xue, W.; Song, B. A.; Yang, S.
573 Synthesis and antibacterial activity of pyridinium-tailored 2,5-
574 substituted-1,3,4-oxadiazole thioether/sulfoxide/sulfone derivatives. *Bioorg. Med.*
575 *Chem. Lett.* **2016**, *26*, 1214-1217.
576 (6) Li, P.; Hu, D. Y.; Xie, D. D.; Chen, J. X.; Jin, L. H.; Song, B. A. Design,
577 Synthesis, and Evaluation of New Sulfone Derivatives Containing a
578 1,3,4-Oxadiazole Moiety as Active Antibacterial Agents. *J. Agric. Food Chem.*

579 **2018**, *66*, 3093-3100.

580 (7) Zhou, J.; Tao, Q. Q.; Wang, P. Y.; Shao, W. B.; Wu, Z. B.; Li, Z.; Yang, S.
581 Antimicrobial evaluation and action mechanism of pyridinium-decorated
582 1,4-pentadien-3-one derivatives. *Bioorg. Med. Chem. Lett.* **2018**, *28*, 1742-1746.

583 (8) Głuszyn´ ska, A. Biological potential of carbazole derivatives. *Eur. J. Med.*
584 *Chem.* **2015**, *94*, 405-426.

585 (9) Zhang, F. F.; Gan, L. L.; Zhou, C. H. Synthesis, antibacterial and antifungal
586 activities of some carbazole derivatives. *Bioorg. Med. Chem. Lett.* **2010**, *20*,
587 1881-1884.

588 (10) Wang, P. Y.; Fang, H. S.; Shao, W. B.; Zhou, J.; Chen, Z.; Song, B. A.; Yang, S.
589 Synthesis and biological evaluation of pyridinium-functionalized carbazole
590 derivatives as promising antibacterial agents. *Bioorg. Med. Chem. Lett.* **2017**, *27*,
591 4294-4297.

592 (11) Huang, Y. Q.; Guo, Z. L.; Song, H. J., Liu, Y. X.; Wang, L. Z.; Wang, Q. M.
593 Design, synthesis, and biological activity of β-carboline analogues containing
594 hydantoin, thiohydantoin, and urea moieties. *J. Agric. Food Chem.* **2018**, *66*,
595 8253-8261.

596 (12) Su, X. L.; Xu, S.; Shan, Y.; Yin, M.; Chen, Y.; Feng, X.; Wang, Q. Z. Three new
597 quinazolines from *Evodia rutaecarpa* and their biological activity. *Fitoterapia*
598 **2018**, *127*, 186-192.

599 (13) Cheng, C. Y.; Chang, C. P.; Yang Lauderdale, T. L.; Yu, G. Y.; Lee, J. C.; Jhang,
600 Y. W.; Wu, C. H.; Ke, Y. Y.; Sadani, A. A.; Yeh, C. F.; Huang, I. W.; Kuo, Y. P.;

601 Tsai, D. J.; Yeh, T. K.; Tseng, C. T.; Song, J. S.; Liu, Y. W.; Tsou, L. K.; Shia, K.
602 S. Bromomethylthioindole inspired carbazole hybrids as promising class of
603 Anti-MRSA agents. *ACS Med. Chem. Lett.* **2016**, *7*, 1191-1196.
604 (14) Zhang, Y.; Tangadanchu, V. K. R.; Bheemanaboina, R. R. Y.; Cheng, Y.; Zhou,
605 C. H. Novel carbazole-triazole conjugates as DNA-targeting membrane active
606 potentiators against clinical isolated fungi. *Eur. J. Med. Chem.* **2018**, *155*,
607 579-589.
608 (15) Niu, F. F.; Liu, Y. H.; Jing, Z. P.; Han, G. J.; Sun, L. Q.; Yan, L.; Zhou, L. P.;
609 Wu, Y. B.; Xu, Y.; Hu, L. X.; Zhao, X. H. Novel carbazole sulfonamide
610 microtubule-destabilizing agents exert potent antitumor activity against
611 esophageal squamous cell carcinoma. *Cancer Lett.* **2018**, *420*, 60-71.
612 (16) Vlaar, C. P.; Castillo-Pichardo, L.; Medina, J. I.; Marrero-Serra, C. M.; Vélez, E.;
613 Ramos, Z.; Hernández, E. Design, synthesis and biological evaluation of new
614 carbazole derivatives as anti-cancer and anti-migratory agents. *Bioorg. Med.*
615 *Chem.* **2018**, *26*, 884-890.
616 (17) Liu, L. X.; Wang, X. Q.; Zhou, B.; Yang, L. J.; Li, Y.; Zhang, H. B.; Yang, X. D.
617 Synthesis and antitumor activity of novel *N*-substituted carbazole imidazolium
618 salt derivatives. *Sci. Rep. -UK* **2015**, *5*, 13101-13120.
619 (18) Pieroni, M.; Girmay, S.; Sun, D. Q.; Sahu, R.; Tekwani, B. L.; Tan, G. T.
620 Synthesis and Structure–Activity Relationships of Lansine Analogues as
621 Antileishmanial Agents. *Chem. Med. Chem.* **2012**, *7*, 1895-1900.
622 (19) Bringmann, G.; Ledermann, A.; Holenz, J.; Kao, M. T.; Busse, U.; Wu, H. G.;
623 Francois, G. Antiplasmodial Activity of Mono- and Dimeric Carbazoles. *Planta*

624 *Med.* **1998**, *64*, 54-57.

625 (20) Saturnino, C.; Grande, F.; Aquaro, S.; Caruso, A.; Iacopetta, D.; Bonomo, M. G.;
626 Longo, P.; Schols, D.; Sinicropi, M. S. Chloro-1,4-dimethyl-9*H*-carbazole
627 Derivatives Displaying Anti-HIV Activity. *Molecules* **2018**, *23*, 286-293.

628 (21) Wang, G. C.; Wang, J.; He, D. X.; Li, X.; Li, J.; Peng, Z. Y. Synthesis and
629 biological evaluation of novel 1,2,4-triazine derivatives bearing carbazole moiety
630 as potent α-glucosidase inhibitors. *Bioorg. Med. Chem. Lett.* **2016**, *26*,
631 2806-2809.

632 (22) Iqbal, S.; Khan, M. A.; Javaid, K.; Sadiq, R.; Fazal-ur-Rehman, S.; Choudhary,
633 M. I.; Basha, F. Z. New carbazole linked 1,2,3-triazoles as highly potent
634 non-sugar α-glucosidase inhibitors. *Bioorg. Chem.* **2017**, *74*, 72-81.

635 (23) Shen, D. Y.; Chan, Y. Y.; Hwang, T. L.; Juang, S. H.; Huang, S. C.; Kuo, P. C.;
636 Thang, T. D.; Lee, E. J.; Damu, A. G.; Wu, T. S. Constituents of the roots of
637 *Clausena lansium* and their potential antiinflammatory activity. *J. Nat. Prod.*
638 **2014**, *77*, 1215-1223.

639 (24) Xia, H. M.; Ou Yang, G. Q.; Li, C. J.; Yang, J. Z.; Ma, J.; Zhang, D.; Li, Y.; Li,
640 L.; Zhang, D. M. Clauemarazoles A-G, seven carbazole alkaloids from the stems
641 of *Clausena emarginata*. *Fitoterapia* **2015**, *103*, 83-89.

642 (25) Molette, J.; Routier, J.; Abla, N.; Besson, D.; Bombrun, A.; Brun, R.; Burt, H.;
643 Georgi, K.; Kaiser, M.; Nwaka, S.; Muzerelle, M; Scheer, A. Identification and
644 optimization of an aminoalcohol-carbazole series with antimalarial properties.
645 *ACS Med. Chem. Lett.* **2013**, *4*, 1037-1041.

646 (26) Indumathi, T.; Fronczek, F. R.; Prasad, K. J. R. Synthesis of
647 2-amino-8-chloro-4-phenyl-5,11-dihydro-6H-pyrido[2,3-a]carbazole-3-carbonitril
648 e: Structural and biological evaluation. *J. Mol. Struct.* **2012**, *1016*, 134-139.
649 (27) Humphries, P. S.; Bersot, R.; Kincaid, J.; Mabery, E.; Mccluskie, K.; Park, T.;
650 Renner, T.; Riegler, E.; Steinfeld, T.; Turtle, E. D.; Wei, Z. L.; Willis, E.
651 Carbazole-containing amides and ureas: discovery of cryptochrome modulators as
652 antihyperglycemic agents. *Bioorg. Med. Chem. Lett.* **2018**, *28*, 293-297.
653 (28) Patel, O. P. S.; Mishra, A.; Maurya, R.; Saini, D.; Pandey, J.; Taneja, I.; Raju, K.
654 S. R.; Kanojiya, S.; Shukla, S. K.; Srivastava, M. N.; Wahajuddin, M.; Tamrakar,
655 A. K.; Srivastava, A. K.; Yadav, P. P. Naturally Occurring Carbazole Alkaloids
656 from *Murraya koenigii* as Potential Antidiabetic Agents. *J. Nat. Prod.* **2016**, *79*,
657 1276-1284.
658 (29) MacMillan, K. S.; Naidoo, J.; Liang, J.; Melito, L.; Williams, N. S.; Morlock, L.;
659 Huntington, P. J.; Estill, S. J.; Longgood, J.; Becker, G. L.; McKnight, S. L.;
660 Pieper, A. A.; Brabander, J. K. D.; Ready, J. M. Development of Proneurogenic,
661 Neuroprotective Small Molecules. *J. Am. Chem. Soc*. **2011**, *133*, 1428-1437.
662 (30) Pieper, A. A.; Xie, S.; Capota, E.; Estill, S. J.; Zhong, J.; Long, J. M.; Becker, G.
663 L.; Huntington, P.; Goldman, S. E.; Shen, C. H.; Capota, M.; Britt, J. K.; Kotti,
664 T.; Ure, K.; Brat, D. J.; Williams, N. S.; MacMillan, K. S.; Naidoo, J.; Melito, L.;
665 Hsieh, J.; De Brabander, J.; Ready, J. M.; McKnight, S. L. Discovery of a
666 proneurogenic, neuroprotective chemical. *Cell* **2010**, *142*, 39-51.
667 (31) Ghobadian, R.; Nadri, H.; Moradi, A.; Bukhari, S. N. A.; Mahdavi, M.; Asadi, M.;

668 Akbarzadeha, T.; Khaleghzadeh-Ahangar, H.; Sharifzadeh, M.; Amini, M. Design,
669 synthesis, and biological evaluation of selective and potent Carbazole-based
670 butyrylcholinesterase inhibitors. *Bioorg. Med. Chem.* **2018**, *26*, 4952-4962.
671 (32) Bertini, S.; Ghilardi, E.; Asso, V.; Minutolo, F.; Rapposelli, S.; Digiacomo, M.;
672 Saccomanni, G; Salmaso, V.; Sturlese, M.; Moro, S.; Macchia, M.; Manera, C.
673 Sulfonamido-derivatives of unsubstituted carbazoles as BACE1 inhibitors.
674 *Bioorg. Med. Chem. Lett.* **2017**, *27*, 4812-4816.
675 (33) Bertini, S.; Asso, V.; Ghilardi, E.; Granchi, C.; Manera, C.; Minutolo, F.;
676 Saccomanni, G.; Bortolato, A.; Mason, J.; Moro, S.; Macchia, Marco.
677 Carbazole-containing arylcarboxamides as BACE1 inhibitors. *Bioorg. Med.*
678 *Chem. Lett.* **2011**, *21*, 6657-6661.
679 (34) Bashir, M.; Bano, A.; Ijaz, A. S.; Chaudhary, B. A. Recent Developments and
680 Biological Activities of *N*-Substituted Carbazole Derivatives: A Review.
681 *Molecules* **2015**, *20*, 13496-13517.
682 (35) Chakraborty, A.; Chowdhury, B. K.; Bhattacharyya, P. Clausenol and
683 clausenine-two carbazole alkaloids from *Clausena anisata*. *Phytochemistry* **1995**,
684 *40*, 295-298.
685 (36) Chakrabarty, M.; Nath, A. C.; Khasnobis, S.; Chakrabarty, M.; Konda, Y.;
686 Harigaya, Y.; Komiyama, K. Carbazole alkaloids from Murraya koenigii.
687 *Phytochemistry*, **1997**, *46*, 751-755.
688 (37) Surineni, G.; Yogeeswari, P.; Sriram, D.; Kantevari, S. Design and synthesis of
689 novel carbazole tethered pyrrole derivatives as potent inhibitors of

690 mycobacterium tuberculosis. *Bioorg. Med. Chem. Lett.* **2015**, *25*, 485-491.

691 (38) Jiang, H.; Zhang, W. J.; Li, P. H.; Wang, J.; Dong, C. Z.; Zhang, K.; Chen, H. X.;
692 Du, Z. Y. Synthesis and biological evaluation of novel carbazole-rhodanine
693 conjugates as topoisomerase II inhibitors. *Bioorg. Med. Chem. Lett.* **2018**, *28*,
694 1320-1323.

695 (39) Yoon, S.; Kim, J. H.; Lee, Y. J.; Ahn, M. Y.; Choi, G.; Kim, W. K.; Yang, Z.;
696 Lee, H. J.; Moon, H. R.; Kim, H. S. A novel carbazole derivative, MHY407,
697 sensitizes cancer cells to doxorubicin-, etoposide-, and radiation treatment via
698 DNA damage. *Eur. J. Pharmacol.* **2012**, *697*, 24-31.

699 (40) Ngo, H. P. T.; Ho, T. H.; Lee, I.; Tran, H. T.; Sur, B.; Kim, S.; Kim, J. G.; Ahn,
700 Y. J.; Cha, S. S.; Kang, L. W. Crystal Structures of Peptide Deformylase from
701 Rice Pathogen *Xanthomonas oryzae pv. oryzae* in Complex with Substrate
702 Peptides, Actinonin, and Fragment Chemical Compounds. *J. Agric. Food Chem.*
703 **2016**, *64*, 7307-7314.

704 (41) Piazza, A.; Zimaro, T.; Garavaglia, B. S.; Ficarra, F. A.; Thomas, L.;
705 Marondedze, C.; Feil, R.; Lunn, J. E.; Gehring, C.; Ottado, J.; Gottig, N. The dual
706 nature of trehalose in citrus canker disease: a virulence factor for *xanthomonas*
707 *citri subsp. citri* and a trigger for plant defence responses. *J. Exp. Bot.* **2015**, *66*,
708 2795-2811.

709 (42) Schaad, N. W.; Wang, Z. K.; Di, M.; McBeath, J.; Peterson, G. L.; Bonde, M. R.
710 An improved infiltration technique to test the pathogenicity of *Xanthomonas*
711 *oryzae pv. oryzae* in rice seedlings. *Seed Sci. Technol.* **1996**, *24*, 449-456.

712 (43) Gao, M. N.; Yu, L.; Li, P.; Song, X. P.; Chen, Z.; He, M.; Song, B. A. Label-free
713 quantitative proteomic analysis of inhibition of *Xanthomonas axonopodis pv. citri*
714 by the novel bactericide Fubianezuofeng. *Pestic. Biochem. Physi.* **2017**, *138*,
715 37-42.
716 (44) Song, X. P.; Li, P.; Li, M. W.; Yang, A. M.; Yu, L.; Luo, L. G.; Hu, D. Y.; Song,
717 B. A. Synthesis and investigation of the antibacterial activity and action
718 mechanism of 1,3,4-oxadiazole thioether derivatives. *Pestic. Biochem. Physiol.*
719 **2018**, *147*, 11-19.
720 (45) Shi, J.; Yu, L.; Song, B. A. Proteomics analysis of xiangcaoliusuobingmi-treated
721 capsicum annuum L. infected with cucumber mosaic virus. *Pestic. Biochem.*
722 *Physiol.* **2018**, *149*, 113-122.
723 (46) Madda, R.; Lin, S. C.; Sun, W. H.; Huang, S. L. Plasma proteomic analysis of
724 systemic lupus erythematosus patients using liquid chromatography/tandem mass
725 spectrometry with label-free quantification. *Peer J* **2018**, *6*, 4730-4742.
726 (47) Kanehisa, M.; Goto, S.; Sato, Y.; Kawashima, M.; Furumichi, M.; Tanabe, M.
727 Data, information, knowledge and principle: back to metabolism in KEGG.
728 *Nucleic Acids Res.* **2014**, *42*, 199-205.
729 (48) Pacheco-Alvarez, D.; Solórzano-Vargas, R. S.; Del Río, A. L. Biotin in
730 metabolism and its relationship to human disease. *Arch. Med. Res.* **2002**, *33*,
731 439-447.
732 (49) Li, J.; Brader, G.; Helenius, E.; Kariola, T.; Palva, E. T. Biotin deficiency causes
733 spontaneous cell death and activation of defense signaling. *Plant J.* **2012,** *70*,

734 315-326.

735 (50) Navin, R. Parallel reaction monitoring: a targeted experiment performed using
736 high resolution and high mass accuracy mass spectrometry. *Int. J. Mol. Sci.* **2015**,
737 *16*, 28566-28581.

738 (51) Tang, B. Z.; Meng, E; Zhang, H. J.; Zhang, X. M. Asgaric, S.; Lin, Y. P.; Lin, Y.
739 Y.; Peng, Z. Q.; Qiao, T.; Zhang, X. F.; Hou, Y. M. Combination of label-free
740 quantitative proteomics and transcriptomics reveals intraspecific venom variation
741 between the two strains of Tetrastichus brontispae, a parasitoid of two invasive
742 beetles. *J. Proteomics* **2019**, *192*, 37-53.

743 (52) MacLean, B.; Tomazela, D. M.; Shulman, N.; Chambers, M.; Finney, G. L.;
744 Frewen, B.; Kern, R.; Tabb, D. L.; Liebler, D. C.; MacCoss, M. J. Skyline: an
745 open source document editor for creating and analyzing targeted proteomics
746 experiments. *Bioinformatics* **2010**, *26*, 966-968.

747

748 **Figure captions**

749 **Figure 1.** a) Some natural antimicrobial structures containing carbazole moieties; b)
750 Design strategy for the target molecules.

751 **Figure 2.** Synthetic route for the target molecules **2a**–**2x**.

752 **Figure 3.** Synthetic route for the target molecules **4a–4h**.

753 **Figure 4.** Synthetic route for the target molecules **6a–6d.**

754 **Figure 5.** Curative and protection activities of compound **2f** against rice bacterial leaf
755 blight under greenhouse conditions at 200 μg/mL; **BT** and **TC** were the positive
756 controls at the same conditions.

757 **Figure 6**. a) Box plot of RSD distribution of repeated samples (three repetitions)
758 using quantified proteins; b) Venn diagrams for proteome comparison on control and
759 treatment groups. The blue part is differentially expressed down-regulated proteins,
760 the brown part is up-regulated proteins, and the center is unchanged; c) Volcano plot
761 of the relative protein abundance changes between control and treatment groups. The
762 red and green points are significantly up- and down-regulated proteins, respectively.

763 **Figure 7.** Differential expression proteins between control and treatment groups were
764 classified based on known biological process (A), molecular functions (B), and
765 cellular components (C).

766 **Figure 8.** Starch and sucrose metabolism and biotin metabolism signaling pathways
767 in response to compound **2f**. Red color represents up-accumulated genes or proteins in
768 this pathway, while the blue color represents down accumulation.

769 **Figure 9.** Protein-protein interaction networks for differentially expressed proteins.

770 The circles and different colors in the figure represent the differentially expressed
771 proteins (blue and red respectively represent the down- and the up-regulated proteins).
772 **Figure 10.** Confirmation of 20 selected differentially produced proteins detected by
773 PRM technique.
774 **Figure 11.** Fluorescence spectra for a) time-dependent fluorescent intensity of
775 compound **2f** ($1 \times 10^{-8}$ M) in TRIS -buffer (50 nM, pH = 7.4); b) time-dependent
776 fluorescent intensity of compound **2f** after adding a 1eq. DNA in TRIS-buffer; c)
777 concentration-dependent fluorescent intensity of compound **2f** with different dosages
778 of DNA.
779 **Figure 12.** SEM images for *Xoo*, *Xac* and *Psa* after being incubated with different
780 concentrations of compound **2f**, *Xoo* images for (a) 0 μg/mL, (b) 12.5 μg/mL, and (c)
781 25.0 μg/mL; *Xac* images for (d) 0 μg/mL, (e) 12.5 μg/mL, and (f) 25.0 μg/mL; *Psa*
782 images for (g) 0 μg/mL, (h) 12.5 μg/mL, and (i) 25 μg/mL. Scale bars are 1 μm.
783

784 **Tables**

785 **Table 1.** Antibacterial activities of target compounds **2a-2x** against plant pathogens

786 *Xoo*, *Xac*, and *Psa in vitro*.

| Compd. | *Xoo* | | *Xac* | | *Psa* | |
|---|---|---|---|---|---|---|
| | Regression equation | $EC_{50}$ (μg/mL) | Regression equation | $EC_{50}$ (μg/mL) | Regression equation | $EC_{50}$ (μg/mL) |
| **2a** | y = 3.650x + 3.357 | 2.82 ± 0.09 | y = 2.883x + 4.136 | 1.99 ± 0.03 | y = 1.019x + 4.742 | 1.79 ± 0.35 |
| **2b** | y = 5.573x + 4.000 | 1.51 ± 0.03 | y = 4.085x + 3.958 | 1.80 ± 0.04 | y = 3.919x + 2.759 | 3.73 ± 0.09 |
| **2c** | y = 8.939x + 1.059 | 2.76 ± 0.02 | y = 2.214x + 4.133 | 2.46 ± 0.09 | y = 1.804x + 3.925 | 3.94 ± 0.07 |
| **2d** | y = 1.482x + 3.506 | 10.2 ± 0.5 | y = 0.720x + 4.349 | 8.01 ± 0.63 | / | >100 |
| **2e** | y = 8.837x + 3.747 | 1.39 ± 0.01 | y = 2.353x + 4.382 | 1.83 ± 0.05 | y = 4.619x + 1.129 | 6.88 ± 0.04 |
| **2f** | y = 14.74x + 3.46 | 1.27 ± 0.01 | y = 4.418x + 3.713 | 1.96 ± 0.03 | y = 4.461x + 2.400 | 3.83 ± 0.05 |
| **2g** | y = 4.149x - 1.428 | 35.4 ± 0.5 | y = 4.581x - 1.801 | 30.5 ± 1.2 | y =2.065x + 1.959 | 29.7 ± 1.7 |
| **2h** | y = 5.985x + 1.209 | 4.30 ± 0.02 | y = 1.450x + 4.610 | 1.86 ± 0.05 | y=1.229x + 3.961 | 7.01 ± 0.38 |
| **2i** | y = 11.73x + 1.346 | 2.05 ± 0.02 | y = 1.343x + 4.652 | 1.81 ± 0.15 | / | >100 |
| **2j** | y = 3.763x + 3.834 | 2.04 ± 0.03 | y = 2.006x + 4.229 | 2.42 ± 0.05 | y = 0.388x + 5.085 | 0.603 ± 0.292 |
| **2k** | y = 10.16x + 1.481 | 2.22 ± 0.04 | y = 2.311x + 4.063 | 2.54 ± 0.18 | y = 2.479x + 2.607 | 9.24 ± 0.06 |
| **2l** | y = 12.80x - 5.574 | 6.70 ± 0.04 | y = 0.961x + 4.693 | 2.08 ± 0.12 | y = 1.129x + 4.359 | 3.70 ± 0.21 |
| **2m** | y = 3.544x + 2.492 | 5.10 ± 0.12 | y = 0.850x + 4.475 | 4.15 ± 0.18 | / | >100 |
| **2n** | y = 4.058x + 3.727 | 2.06 ± 0.08 | y = 2.326x + 3.224 | 5.80 ± 0.14 | y = 0.492x + 4.577 | 7.23 ± 0.78 |
| **2o** | / | >100 | / | >100 | / | >100 |
| **2p** | / | >100 | / | >100 | y = 1.493x + 3.378 | 12.2 ± 0.1 |
| **2q** | / | >100 | / | >100 | / | >100 |
| **2r** | / | >100 | / | >100 | y = 0.660x + 4.007 | 32.0 ± 1.3 |
| **2s** | y = 3.345x + 1.494 | 11.2 ± 0.4 | y = 1.609x + 3.458 | 9.08 ± 0.38 | y = 1.211x + 4.094 | 5.60 ± 0.20 |
| **2t** | y = 7.091x - 4.347 | 20.8 ± 0.5 | y = 1.661x + 3.828 | 5.07 ± 0.33 | y = 2.242x + 2.058 | 20.5 ± 1.0 |
| **2u** | y = 10.83x - 9.844 | 23.5 ± 0.4 | y = 2.311x + 2.672 | 10.2 ± 0.8 | y = 1.265x + 3.340 | 20.5 ± 2.6 |
| **2v** | y = 5.837x + 1.748 | 14.3 ± 0.1 | y = 1.117x + 4.178 | 5.44 ± 0.54 | y = 0.849x + 4.397 | 5.14 ± 0.02 |
| **2w** | y = 3.345x + 3.931 | 2.09 ± 0.04 | y = 2.220x + 4.382 | 1.90 ± 0.06 | y = 0.696x + 4.523 | 4.84 ± 0.22 |

| | | | | | | |
|---|---|---|---|---|---|---|
| **2x** | y = 9.773x + 3.458 | 7.34 ± 0.13 | y = 0.763x + 4.163 | 12.5 ± 2.04 | y = 0.867x + 4.355 | 5.55 ± 0.53 |
| **BT** | y = 1.499x + 2.052 | 92.6 ± 2.1 | / | / | y = 4.913x - 4.246 | 111.2 ± 4.9 |
| **TC** | y = 1.540x + 1.788 | 121.8 ± 3.6 | y = 2.153x + 0.938 | 77.0 ± 2.0 | y = 5.669x - 5.994 | 87.0 ± 2.1 |

787

788 **Table 2.** Antibacterial activities of target compounds **4a–4h** against plant pathogens

789 *Xoo*, *Xac*, and *Psa in vitro*.

| Compd. | *Xoo* | | *Xac* | | *Psa* | |
|---|---|---|---|---|---|---|
| | Regression equation | $EC_{50}$ (μg/mL) | Regression equation | $EC_{50}$ (μg/mL) | Regression equation | $EC_{50}$ (μg/mL) |
| **4a** | y = 1.186x + 3.513 | 17.9 ± 0.3 | / | >100 | / | >100 |
| **4b** | y = 3.208x + 0.990 | 17.2 ± 0.4 | / | >100 | / | >100 |
| **4c** | y = 9.455x + 4.627 | 1.10 ± 0.01 | y = 4.378x + 4.085 | 1.62 ± 0.06 | / | >100 |
| **4d** | y = 9.696x + 3.354 | 1.47 ± 0.02 | y = 5.977x + 2.709 | 2.42 ± 0.01 | / | >100 |
| **4e** | y = 15.14x + 0.579 | 1.96 ± 0.01 | y = 3.776x + 4.482 | 1.37 ± 0.05 | / | >100 |
| **4f** | y = 10.13 x + 3.772 | 1.32 ± 0.02 | y = 5.150x + 4.115 | 1.49 ± 0.01 | / | >100 |
| **4g** | y = 3.340x - 0.634 | 20.3 ± 0.4 | y = 3.746x + 0.188 | 24.3 ± 0.8 | / | >100 |
| **4h** | y = 4.202x - 0.242 | 17.7 ± 0.4 | y = 5.877x + 1.018 | 10.6 ± 0.3 | / | >100 |
| **BT** | y = 1.499x + 2.052 | 92.6 ± 2.1 | / | / | y = 4.913x - 4.246 | 111.2 ± 4.9 |
| **TC** | y = 1.540x + 1.788 | 121.8 ± 3.6 | y = 2.153x + 0.938 | 77.0 ± 2.0 | y = 5.669x - 5.994 | 87.0 ± 2.1 |

790

791 **Table 3.** Antibacterial activities of target compounds **6a–6d** against plant pathogens

792 *Xoo*, *Xac*, and *Psa in vitro*.

| Compd. | *Xoo* | | *Xac* | | *Psa* | |
|---|---|---|---|---|---|---|
| | Regression equation | $EC_{50}$ (μg/mL) | Regression equation | $EC_{50}$ (μg/mL) | Regression equation | $EC_{50}$ (μg/mL) |
| **6a (R)** | y = 17.59x + 2.52 | 1.38 ± 0.03 | y = 1.775x + 3.687 | 5.49 ± 0.08 | / | >100 |
| **6b (S)** | y = 8.457x + 3.475 | 1.51 ± 0.02 | y = 2.939x + 3.552 | 3.11 ± 0.11 | / | >100 |
| **4d (R/S)** | y = 9.696x + 3.354 | 1.47 ± 0.02 | y = 5.977x + 2.709 | 2.42 ± 0.01 | / | >100 |
| **6c (R)** | y = 10.81x + 5.49 | 0.902±0.021 | y = 6.405x + 5.040 | 0.993±0.012 | / | >100 |
| **6d (S)** | y = 4.133x + 4.358 | 1.43 ± 0.04 | y = 8.184x + 4.464 | 1.16 ± 0.02 | / | >100 |
| **4f (R/S)** | y = 10.13x + 3.77 | 1.32 ± 0.02 | y = 5.150x + 4.115 | 1.49 ± 0.01 | / | >100 |
| **BT** | y = 1.499x + 2.052 | 92.6 ± 2.1 | / | / | y = 4.913x-4.246 | 111.2 ± 4.9 |
| **TC** | y = 1.540x + 1.788 | 121.8 ± 3.6 | y = 2.153x + 0.938 | 77.0 ± 2.0 | y = 5.669x-5.994 | 87.0 ± 2.1 |

793

794 **Table 4.** Curative and protection activities of compound **2f** against rice bacterial leaf

795 blight under greenhouse conditions at 200 μg/mL *in vivo*.

| Treatment | Curative activity (14 days after spraying) | | | Protection activity (14 days after spraying) | | |
|---|---|---|---|---|---|---|
| | Morbidity (%) | Disease index (%) | Control efficiency (%)[b] | Morbidity (%) | Disease index (%) | Control efficiency (%)[b] |
| **2f** | 100 | 45.32 | 50.77 | 100 | 47.22 | 48.71 |
| **BT** | 100 | 52.04 | 43.47 | 100 | 54.40 | 40.91 |
| **TC** | 100 | 51.02 | 42.60 | 100 | 54.07 | 39.17 |
| **CK**[a] | 100 | 92.06 | / | 100 | 92.06 | / |

796 [a] Negative control. [b] Statistical analysis was conducted by ANOVA method under the condition of equal variances assumed ($P > 0.05$) and equal variances not assumed ($P < 0.05$). Different uppercase letters indicate the values of protection activity with

797

798 significant difference among different treatment groups at $P < 0.05$.

799

800 **Figures**

801 **Figure 1**

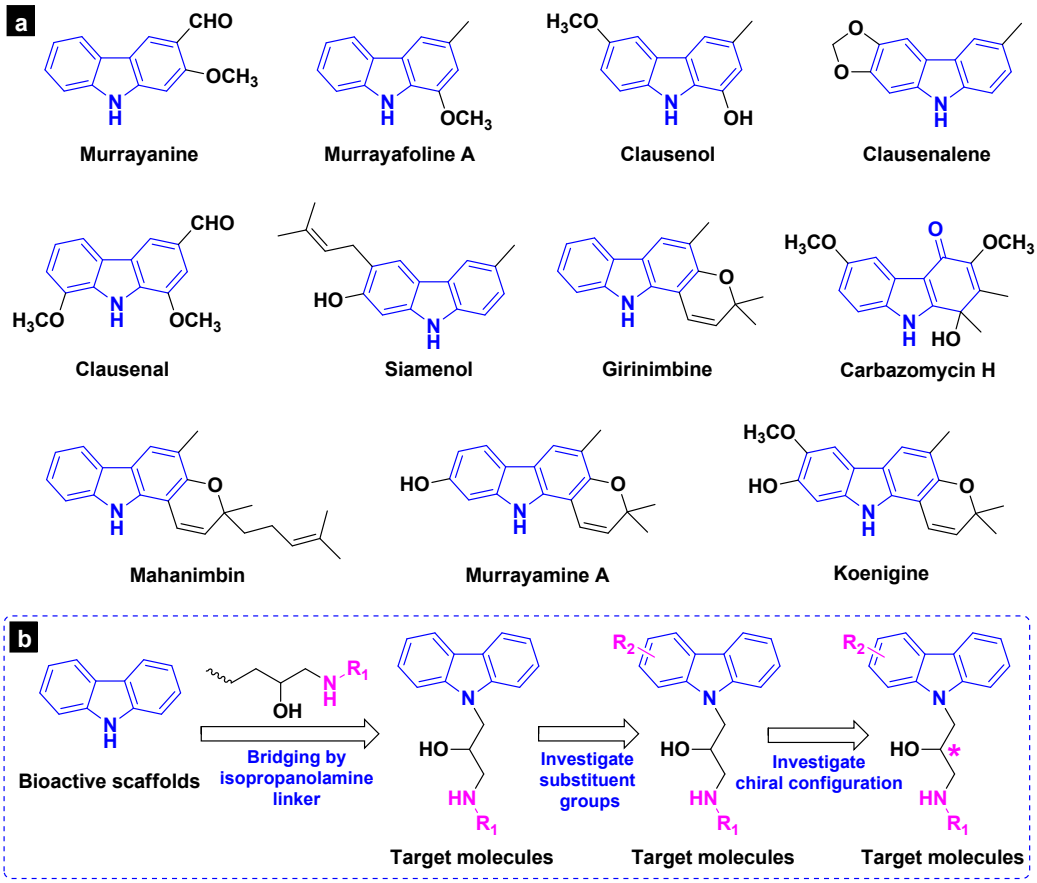


802

803

804 **Figure 2**

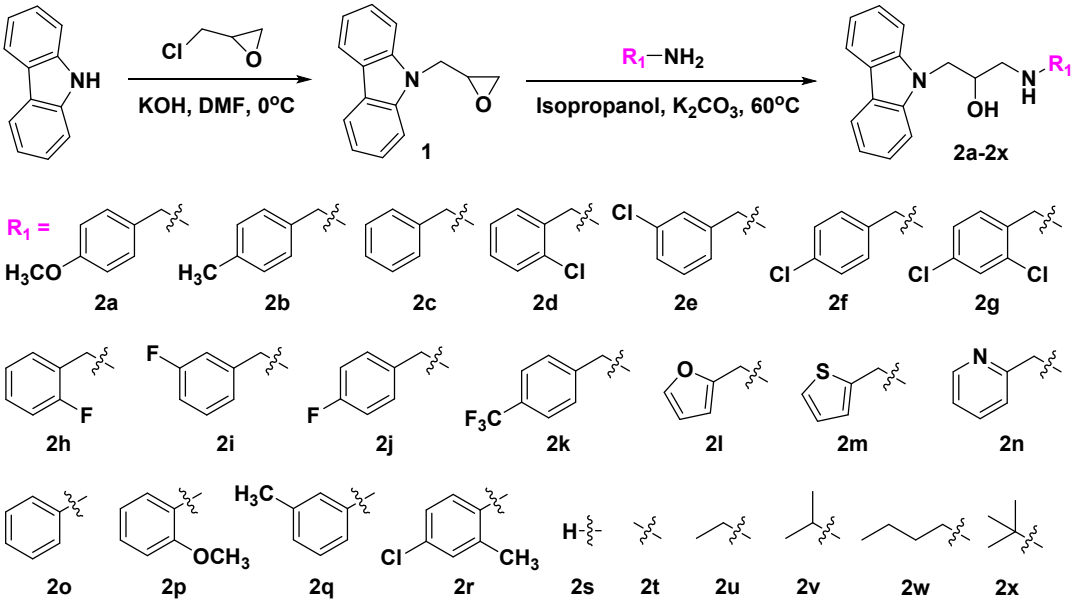


805

806

807 **Figure 3**

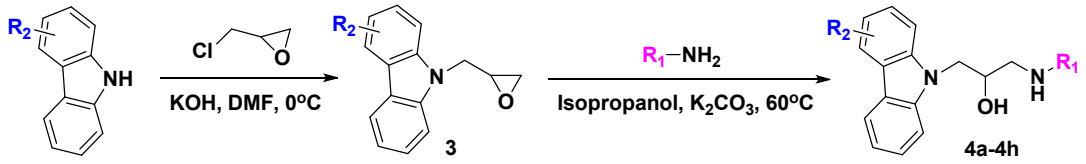


**4a : $R_1$ = 4-chlorobenzyl, $R_2$ = 3,6-diBr**

**4b : $R_1$ = 4-fluorobenzyl, $R_2$ = 3,6-diBr**

**4c : $R_1$ = 4-methylbenzyl, $R_2$ = 3,6-diBr**

**4d : $R_1$ = 4-chlorobenzyl, $R_2$ = 3,6-ditert-butyl**

**4e : $R_1$ = 4-fluorobenzyl, $R_2$ = 3,6-ditert-butyl**

**4f : $R_1$ = 4-methylbenzyl, $R_2$ = 3,6-ditert-butyl**

808 **4g : $R_1$ = 4-chlorobenzyl, $R_2$ = 3,6-diacetyl**

**4h : $R_1$ = 4-methylbenzyl, $R_2$ = 3,6-diacetyl**

809

**Figure 4**

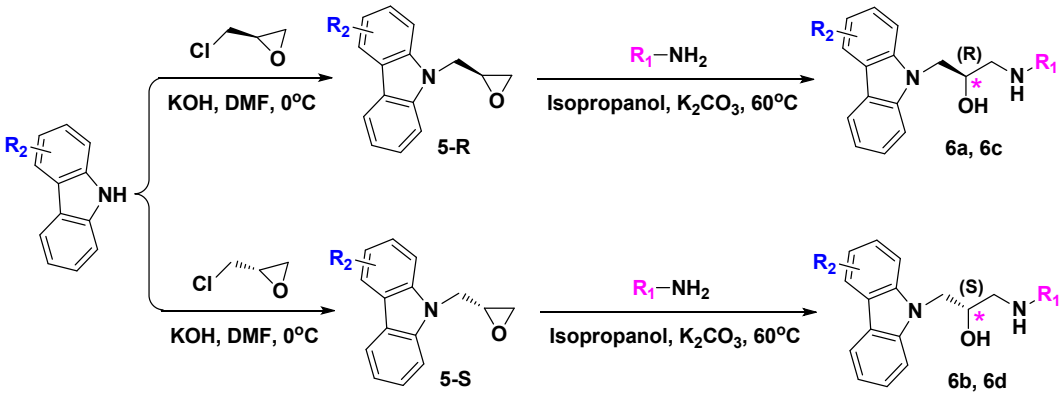


6a: $R_1$ = 4-chlorobenzyl, $R_2$ = 3,6-ditert-butyl

6b: $R_1$ = 4-chlorobenzyl, $R_2$ = 3,6-ditert-butyl

6c: $R_1$ = 4-methylbenzyl, $R_2$ = 3,6-ditert-butyl

6d: $R_1$ = 4-methylbenzyl, $R_2$ = 3,6-ditert-butyl

**Figure 5**


CK
2f
Bismerthiazol
Curative activity
Thiodiazole copper
CK
2f
Bismerthiazol
Protection activity
Thiodiazole copper

**Figure 6**

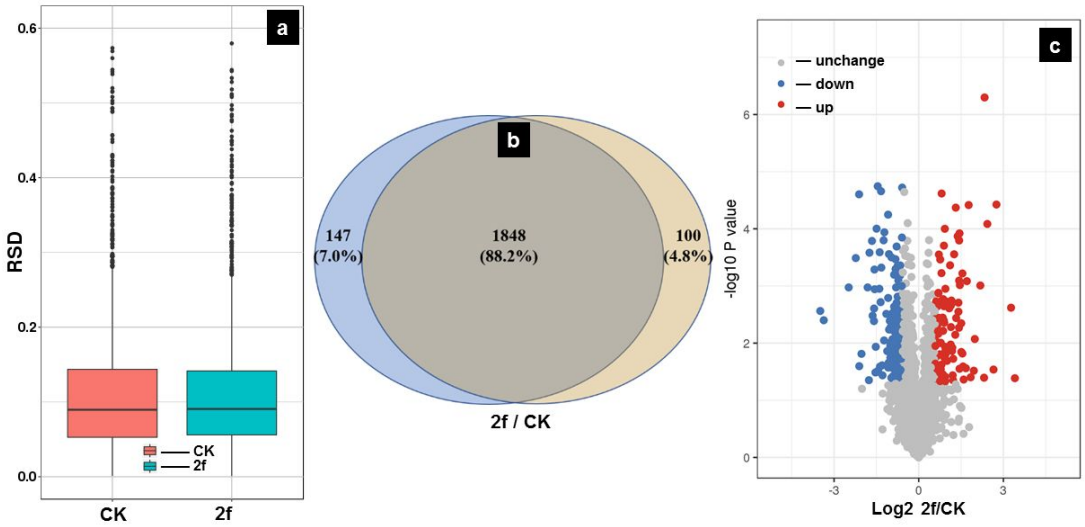
a
RSD
0.6
0.4
0.2
0.0
CK
2f
CK
2f
b
147
(7.0%)
1848
(88.2%)
100
(4.8%)
2f / CK
c
unchange
down
up
-log10 P value
Log2 2f/CK

**Figure 7**

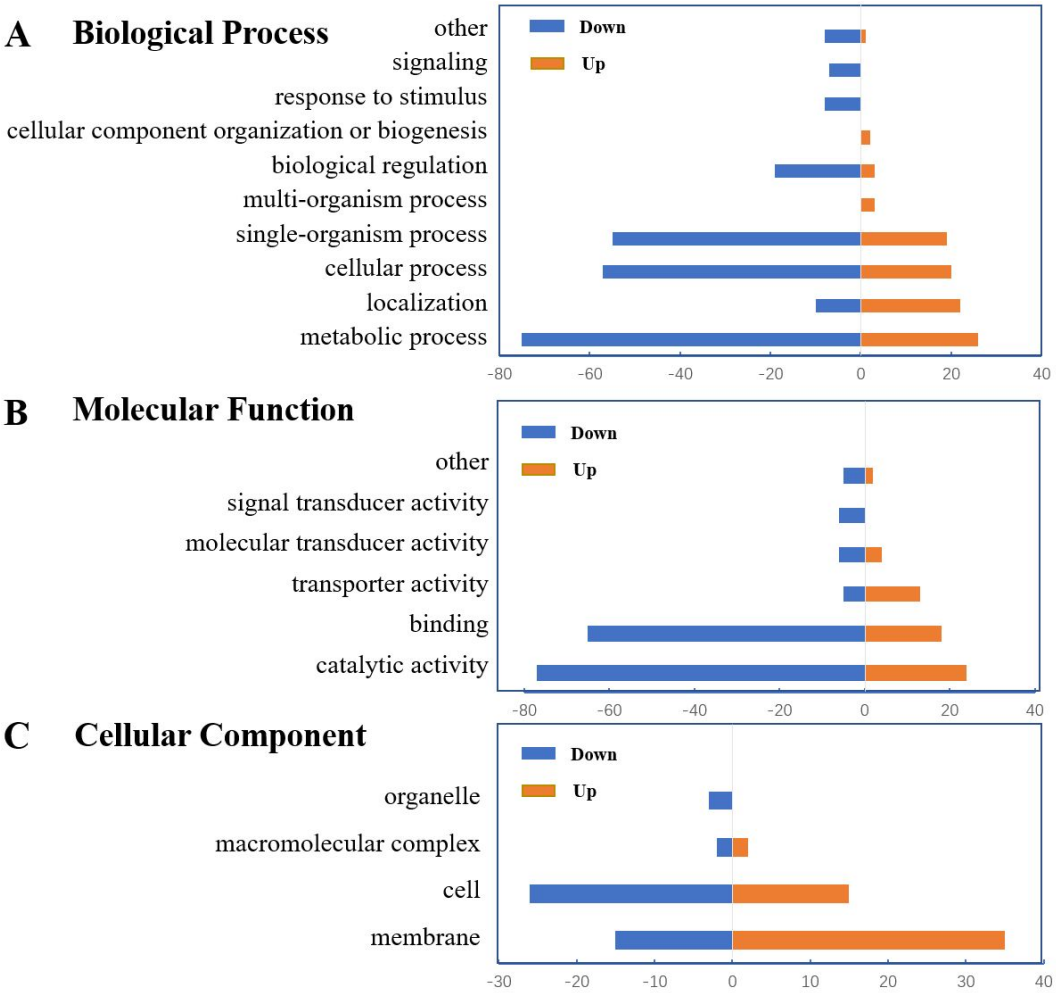
A Biological Process
other
signaling
response to stimulus
cellular component organization or biogenesis
biological regulation
multi-organism process
single-organism process
cellular process
localization
metabolic process
Down
Up
-80 -60 -40 -20 0 20 40
B Molecular Function
other
signal transducer activity
molecular transducer activity
transporter activity
binding
catalytic activity
Down
Up
-80 -60 -40 -20 0 20 40
C Cellular Component
organelle
macromolecular complex
cell
membrane
Down
Up
-30 -20 -10 0 10 20 30 40

822 **Figure 8**

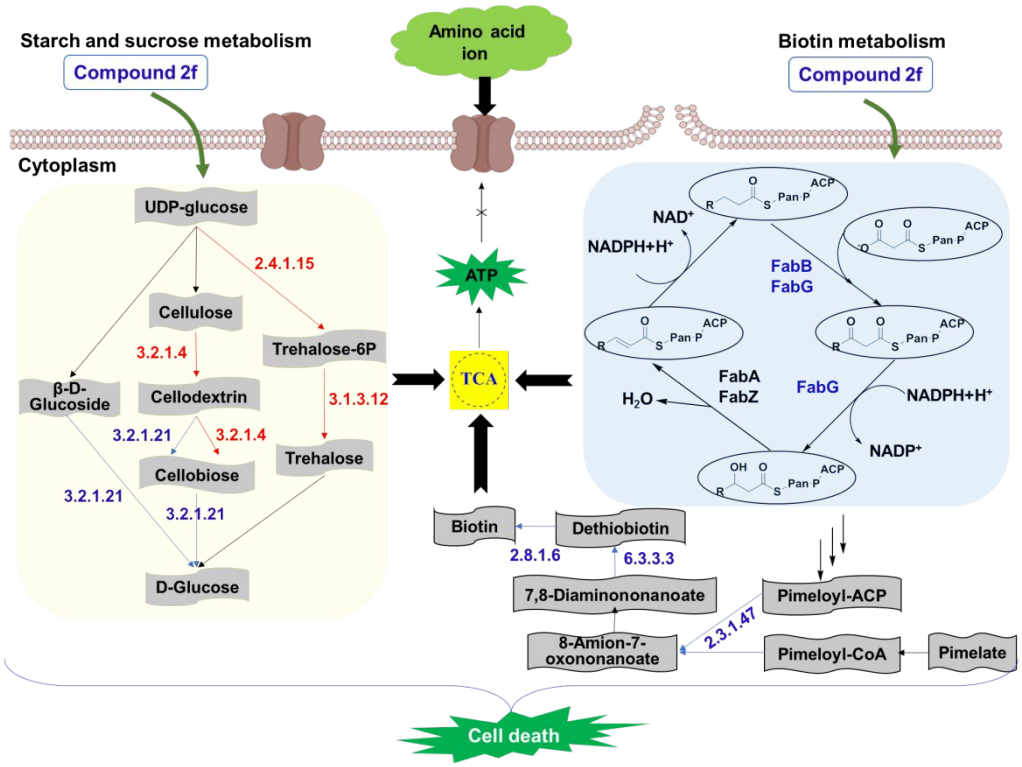


823

824

**Figure 9**

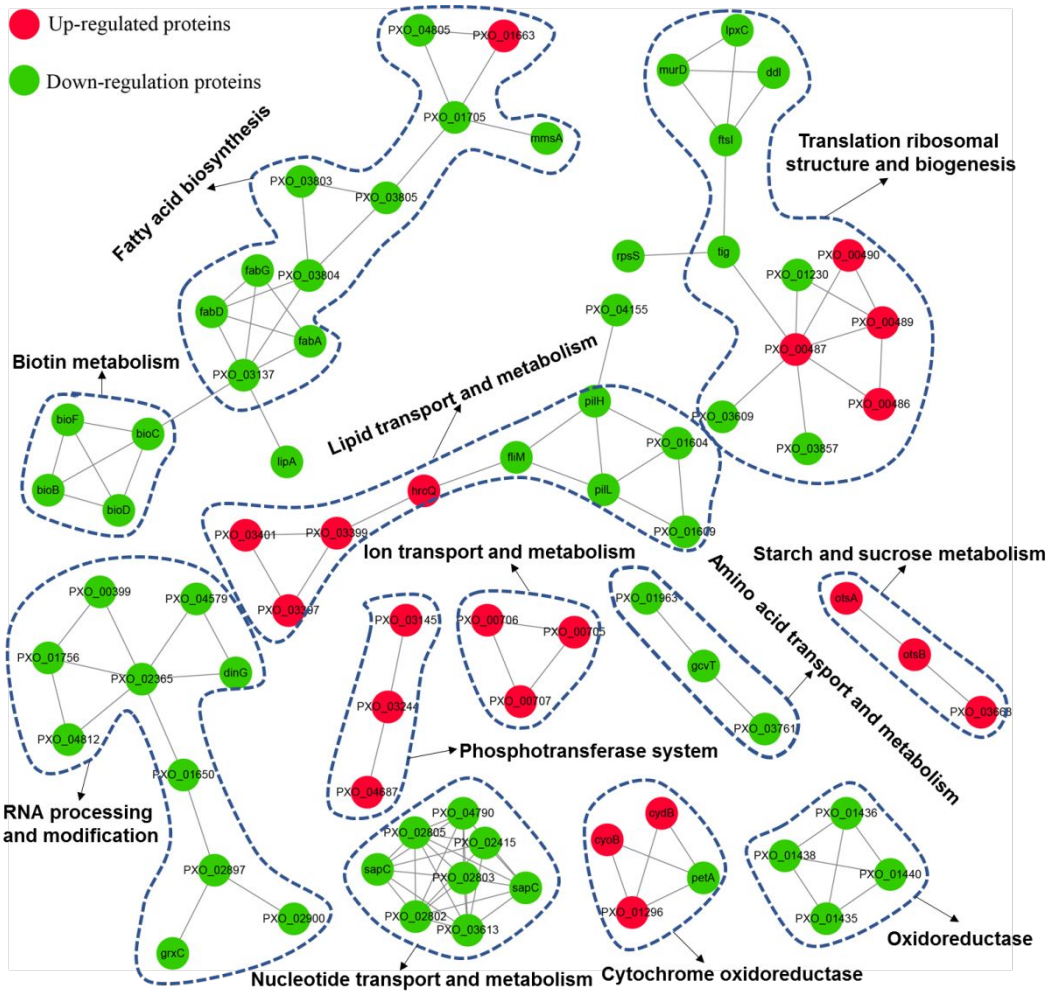
Up-regulated proteins
Down-regulation proteins
Fatty acid biosynthesis
Translation ribosomal structure and biogenesis
Biotin metabolism
Lipid transport and metabolism
Ion transport and metabolism
Starch and sucrose metabolism
Amino acid transport and metabolism
Phosphotransferase system
RNA processing and modification
Nucleotide transport and metabolism
Cytochrome oxidoreductase
Oxidoreductase
PXO_04805
PXO_01663
PXO_01705
mmsA
PXO_03803
PXO_03805
fabG
PXO_03804
fabD
fabA
PXO_03137
lipA
bioF
bioC
bioB
bioD
lpxC
murD
ddl
ftsI
rpsS
tig
PXO_00490
PXO_01230
PXO_00489
PXO_00487
PXO_00486
PXO_03609
PXO_03857
PXO_04155
pilH
PXO_01604
fliM
pilL
PXO_01609
hrcQ
PXO_03401
PXO_03399
PXO_03397
PXO_00399
PXO_04579
PXO_01756
PXO_02365
dinG
PXO_04812
PXO_01650
PXO_02897
PXO_02900
grxC
PXO_03451
PXO_03244
PXO_04687
PXO_00706
PXO_00705
PXO_00707
PXO_01963
gcvT
PXO_03761
otsA
otsB
PXO_03568
PXO_04790
PXO_02805
PXO_02415
sapC
PXO_02803
sapC
PXO_02802
PXO_03613
cydB
cyoB
petA
PXO_01296
PXO_01436
PXO_01438
PXO_01440
PXO_01435

828 **Figure 10**

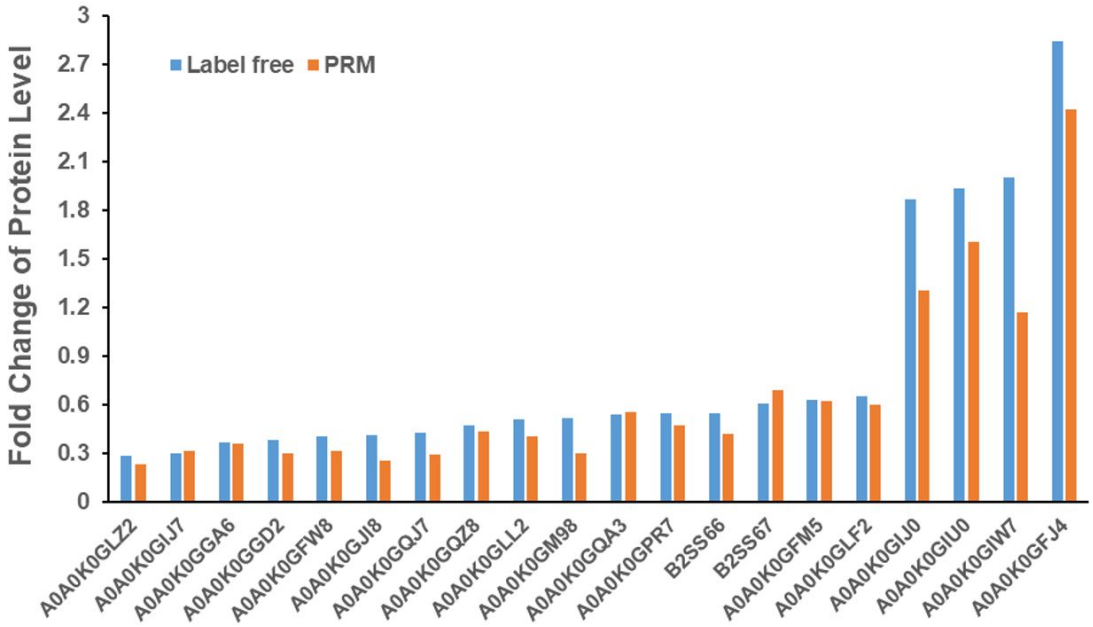


829

830

831 **Figure 11**

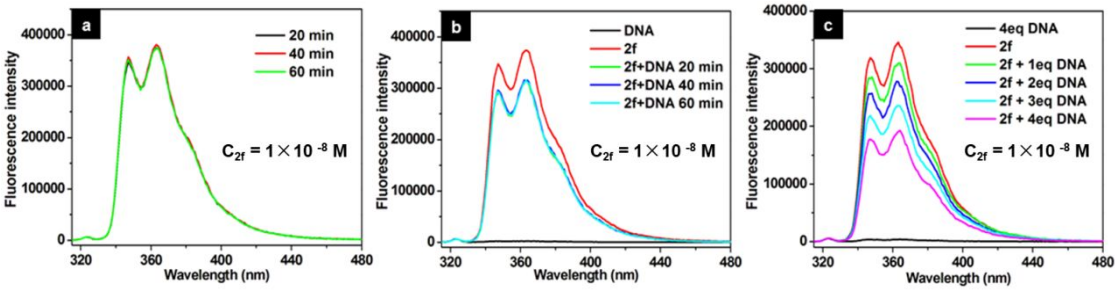


832

833

834 **Figure 12**

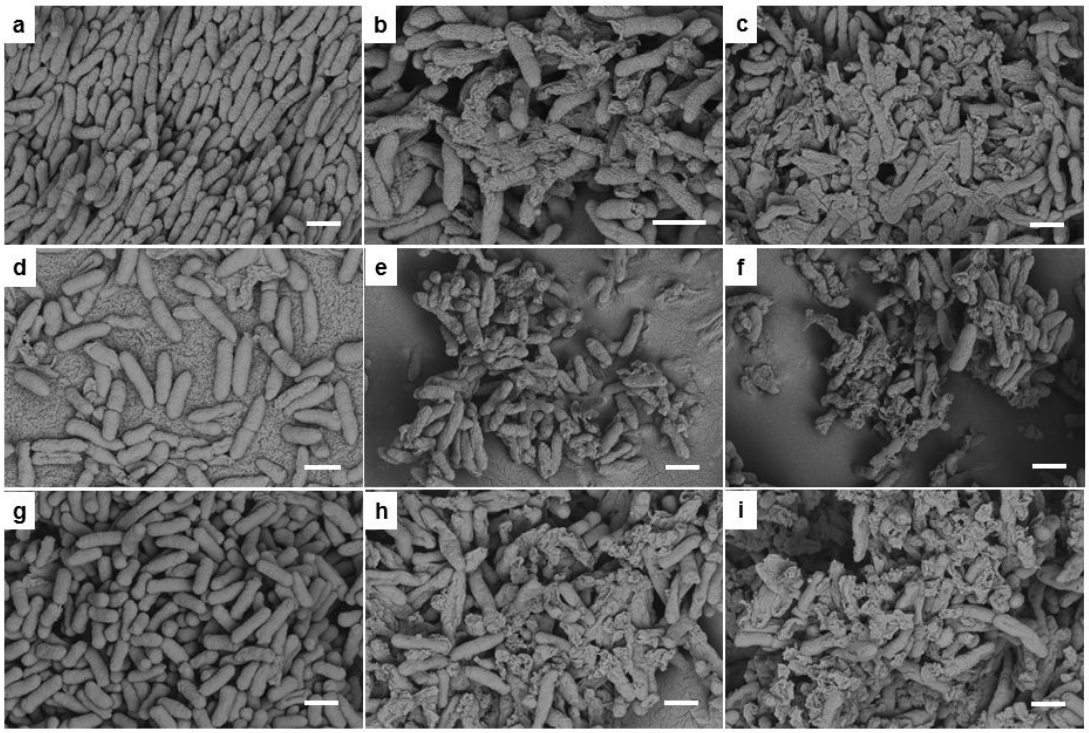


835
836

837 **Graphic for Table of Contents**

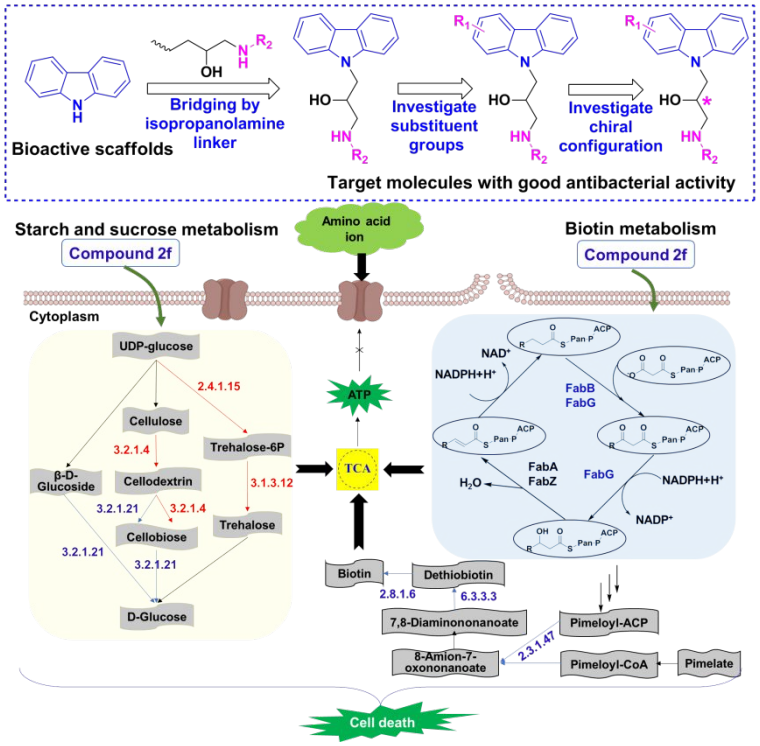


838